



## RESEARCH ARTICLE

10.1029/2019GC008874

### Key Points:

- Refined eruption stratigraphy for Japan (between 50 and 30 ka) through the identification of cryptotephra layers in the varved Lake Suigetsu sediment core
- Aso caldera was particularly active between 35 and 30 ka, producing at least 5 tephra that were dispersed >500 km from source
- A large eruption occurred from Aira 1.3 ka before the cataclysmic VEI 7 caldera-forming AT eruption that blanketed Japan in ash

### Supporting Information:

- Supporting Information S1
- Data Set S1

### Correspondence to:

D. McLean,  
mclean.tephra@gmail.com

### Citation:

McLean, D., Albert, P. G., Suzuki, T., Nakagawa, T., Kimura, J.-I., Chang, Q., et al. (2020). Constraints on the timing of explosive volcanism at Aso and Aira calderas (Japan) between 50 and 30 ka: New insights from the Lake Suigetsu sedimentary record (SG14 core). *Geochemistry, Geophysics, Geosystems*, 21, e2019GC008874. <https://doi.org/10.1029/2019GC008874>

Received 16 DEC 2019

Accepted 10 APR 2020

Accepted article online 8 MAY 2020

## Constraints on the Timing of Explosive Volcanism at Aso and Aira Calderas (Japan) Between 50 and 30 ka: New Insights From the Lake Suigetsu Sedimentary Record (SG14 Core)

D. McLean<sup>1</sup> , P. G. Albert<sup>1,2</sup>, T. Suzuki<sup>3</sup>, T. Nakagawa<sup>4</sup>, J.-I. Kimura<sup>5</sup> , Q. Chang<sup>5</sup>, Y. Miyabuchi<sup>6</sup>, C. J. Manning<sup>7</sup>, A. MacLeod<sup>8,9</sup>, S. P. E. Blockley<sup>8</sup>, R. A. Staff<sup>1,10</sup> , K. Yamada<sup>4</sup> , I. Kitaba<sup>4</sup>, A. Yamasaki<sup>11</sup>, T. Haraguchi<sup>12</sup>, J. Kitagawa<sup>13</sup>, SG14 Project Members<sup>14</sup>, and V. C. Smith<sup>1</sup>

<sup>1</sup>Research Laboratory for Archaeology and the History of Art, University of Oxford, Oxford, UK, <sup>2</sup>Department of Geography, College of Science, Swansea University, Swansea, UK, <sup>3</sup>Department of Geography, Tokyo Metropolitan University, Tokyo, Japan, <sup>4</sup>Research Centre for Palaeoclimatology, Ritsumeikan University, Shiga, Japan, <sup>5</sup>Department of Solid Earth Geochemistry, Japan Agency for Marine-Earth Science and Technology, Yokosuka, Japan, <sup>6</sup>Center for Water Cycle, Marine Environment and Disaster Management, Kumamoto University, Kumamoto, Japan, <sup>7</sup>Department of Earth Science, Royal Holloway University of London, Egham, UK, <sup>8</sup>Department of Geography, Royal Holloway University of London, Egham, UK, <sup>9</sup>Department of Geography and Environmental Science, University of Reading, Reading, UK, <sup>10</sup>Scottish Universities Environmental Research Centre, University of Glasgow, East Kilbride, UK, <sup>11</sup>Fukui Prefectural Satoyama-Satoumi Research Institute, Wakawa, Japan, <sup>12</sup>Osaka City University, Osaka, Japan, <sup>13</sup>Fukui Prefectural Varve Museum, Wakasa, Japan, <sup>14</sup>[www.suigetsu.org](http://www.suigetsu.org)

**Abstract** Volcanoes in the East Asian/Pacific region have been the source of some of the largest magnitude eruptions during the Late Quaternary, and accurately evaluating their eruptive histories is essential for hazard assessments. To overcome difficulties in resolving and precisely dating eruptions in the near-source realm, the high-resolution (varved) sediments of Lake Suigetsu (central Honshu, Japan) were examined for the presence of non-visible (cryptotephra) layers from 50 ka up until the 30 ka Aira-Tanzawa (AT) caldera-forming event of Aira volcano. Cryptotephra layers are four times more frequently preserved than visible markers in the Suigetsu sediments, meaning that this archive provides a unique and unprecedented record of eruptions that were dispersed over the densely populated regions of central Honshu. Major and trace element volcanic glass chemistry is used to fingerprint the ash layers and pinpoint their volcanic origin. Tephra are found throughout the investigated sediments, but the highest abundance of ash fall events are recorded between 39 and 30 ka, capturing a period of intense volcanism at calderas on Kyushu Island (Japan). The augmented Suigetsu tephrostratigraphy records at least seven eruptions from Aso caldera (southern Kyushu) that post-date the widespread ACP-4 Plinian eruption (ca. 50 ka) and four explosive events from Aira (central Kyushu) that occurred leading up to the catastrophic caldera-forming AT eruption (ca. 30 ka).

## 1. Introduction

Volcanoes distributed across the heavily populated East Asian/Pacific region have been the source of some of the largest known caldera-forming events (Simkin & Siebert, 2000), blanketing Japan and the surrounding seas in ash (e.g., Machida & Arai, 2003; Mahony et al., 2016; McLean et al., 2020; Schindlbeck et al., 2018; Smith et al., 2013). Accurately reconstructing the tempo and magnitude of pre-historic eruptions at these volcanoes is an essential component of risk and hazard assessments (Kiyosugi et al., 2015). Unfortunately, the burial, destruction, and subsequent erosion of eruption deposits in near-source areas contribute to an incomplete geological record, hampering our ability to accurately reconstruct eruption histories. Piecing together fragmentary records close to the source volcano is further complicated by the fact that many Japanese volcanoes erupt successive deposits with geochemically very similar compositions (e.g., Kimura et al., 2015; Machida and Arai, 2003; McLean et al., 2018; Smith et al., 2013); consequently, deciphering the true number of events is challenging and can result in an under-recording of eruptions (e.g., Albert et al., 2018). Furthermore, precisely evaluating the tempo and recurrence intervals of past eruptions using

©2020. The Authors.

This is an open access article under the terms of the Creative Commons Attribution License, which permits use, distribution and reproduction in any medium, provided the original work is properly cited.

near-source volcanic successions is difficult, and for many volcanoes in Japan this remains a significant obstacle, particularly at low-K (tholeiitic) and medium-K (calc-alkaline) centers, where mineral phases are largely unsuitable for  $^{40}\text{Ar}/^{39}\text{Ar}$  dating. Consequently, dating such eruptions from the last 50 ka is heavily reliant upon the sporadic discovery of charcoal fragments buried within eruption units that are suitable for  $^{14}\text{C}$  dating.

Fortunately, volcanic ash (tephra) deposits are routinely identified in distal sedimentary (palaeoclimate and archaeological) archives in and around Japan (e.g., Albert et al., 2019; Chen et al., 2019; Furuta et al., 1986; Machida & Arai, 1983, 2003; McLean et al., 2018; Moriwaki et al., 2016), which provide critical insights into the tempo, behavior and ash dispersals of highly explosive volcanism in East Asia. The Lake Suigetsu sedimentary archive provides a key tephrostratotype of explosive events for Japan (e.g., Smith et al., 2013), and the unique high-precision chronology (e.g., Bronk Ramsey et al., 2012) ensures that tephra layers identified in the radiocarbon timeframe are robustly dated. The sediments also preserve numerous non-visible (cryptotephra) layers throughout the sequence (e.g., McLean et al., 2018), which are derived from more distal sources and/or lower magnitude events.

This paper explores the cryptotephra record preserved in the ca. 14 m of the varved (annually laminated) Lake Suigetsu sediments (SG14 core) dated between 50 and 30 ka (Bronk Ramsey et al., 2012; Schlögl et al., 2012; 2018). While much more is known about recent eruptions from the proximal volcanological record, the periodicity and repose intervals during the 50 and 30 ka window are at present poorly understood. During this period, the high-resolution sediments of Lake Suigetsu can provide unprecedented insight into the timing and frequency of large eruptions and their associated ash fall events dispersed over the now heavily populated regions of East Asia. Several large calderas situated downwind of Lake Suigetsu (i.e., those on the Ryukyu-Kyushu arc; Figure 1), and Aira and Aso in particular are thought to have been very active between 50 and 30 ka, based on the record preserved in the proximal volcanic stratigraphies (e.g., Miyabuchi, 2009, 2011; Nagaoka et al., 2001). Despite this, almost no distal ash equivalents have been identified. Currently, most eruption ages established during this period are poorly constrained and are either broadly extrapolated based on their stratigraphic position relative to the ~30 ka Aira-Tanzawa (AT) ash from Aira or radiocarbon dated via palaeosols developed during periods of quiescence. A more thorough eruption chronology can aid our understanding of the behavior of these centers prior-to (e.g., Aira) or following (e.g., Aso) large caldera-forming events.

## 2. Study Site and Potential Tephra Sources

### 2.1. Lake Suigetsu, Central Japan

Lake Suigetsu is the largest of the “Mikata Five Lakes” (covering an area of ca. 4.2 km<sup>2</sup>), located in a small tectonic basin on the western side of the Mikata fault, Honshu Island, central Japan (Figure 1; 35°35′0″N, 135°53′0″E, 0 m above present sea level; Figure 1a). The main tributary is the River Hasu, which enters on the southeast side of Lake Mikata and flows through a narrow channel into Lake Suigetsu (Figure 1b). This unique configuration of the lakes and hydrological setting means that cryptotephra layers are well preserved within the fine and laminated (varved) sediments. Suigetsu is also adequately situated away from the large calderas of Hokkaido and Kyushu and so is not inundated with locally sourced volcanic glass, which would also preclude the identification of cryptotephra layers with low concentrations of glass shards.

The “SG06” sedimentary core (Figure 1a) was extracted from Lake Suigetsu in 2006, with the composite sequence spanning ca. 73.2 m. The SG06 core was obtained from four overlapping boreholes A, B, C, and D, which were situated ca. 20 m apart; (Nakagawa et al., 2012). The lake was re-cored in 2014 (“SG14”), to provide additional material for scientific analysis and to prepare sediments for display at the *Fukui Prefectural Varve Museum*. The sediments were obtained from new boreholes E, F, G, and H, which were located ca. 320 m further east of those from SG06. The SG14 sediments were utilized for the cryptotephra investigations outlined in this study.

### 2.2. Sources of Visible Tephra Dispersed to Lake Suigetsu

Thirty-one visible ash layers (named according to their SG06 Composite Depths [CD]) were originally identified in the SG06 core (McLean et al., 2016; Smith et al., 2011, 2013), most of which originating from arc volcanoes south of Suigetsu, situated in the Kyushu Central and Southern Volcanic region (Kikai, Aira, Aso,

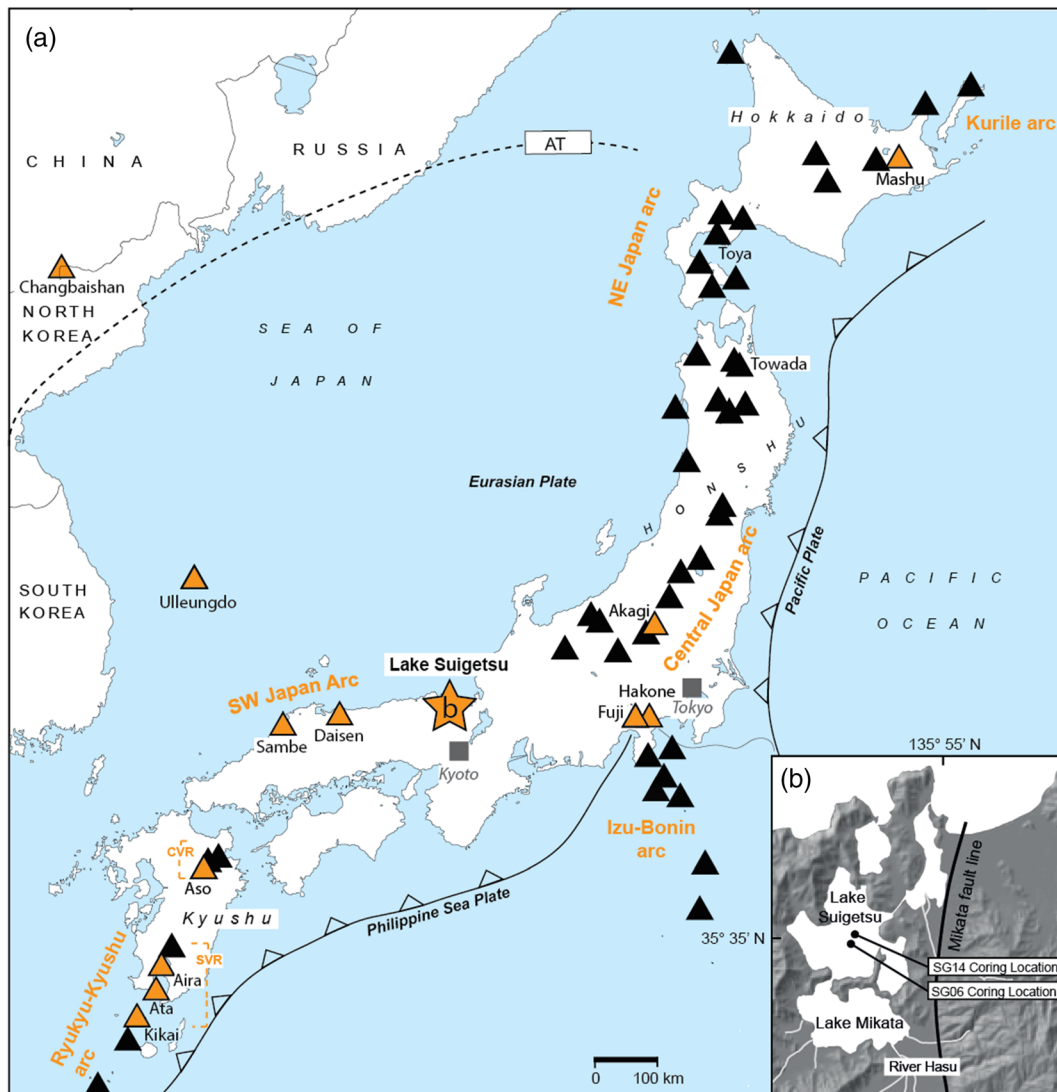


**Figure 1.** (a) Volcanoes in Japan, North Korea/China (Changbaishan) and South Korea (Ulleungdo) (black and orange triangles) known to have been active during the Late Quaternary (data from Machida & Arai, 2003). Volcanoes mentioned within the text are colored orange, and a star denotes the location of Lake Suigetsu. The visible ash dispersal for the AT (Aira volcano; 30 ka) tephra is marked by a dashed line (as defined by Machida & Arai, 2003). (b) Location of the five Mikata lakes, which are situated west of the active Mikata fault, adjacent to Wakasa Bay. The positions of coring campaigns SG06 and SG14 are marked on Lake Suigetsu (modified after Nakagawa et al., 2005).

and Ata volcanoes; Figure 1; see Albert et al., 2019). Four visible tephra layers in the Suigetsu sequence (SG06-0226, SG14-1091, SG06-1288, SG14-3216) originate from intraplate volcanoes Ulleungdo (South Korea) and Changbaishan (North Korea/China) (Figure 1; McLean et al., 2016, 2018, 2020; Smith et al., 2011).

The visible tephrostratigraphic sequence investigated here (50 to 30 ka) is composed of five key markers (see Table 1; Figure 2), which include the Central Pumice Cone 4 (ACP4) eruption from Aso caldera (ca. 50 ka; correlated to Suigetsu tephra SG06-3912), the Ikeda (SI) tephra erupted from Sambe (ca. 46 ka; SG06-3668), an eruption from Ko-Fuji (ca. 44 ka; SG06-3485), the Ulleung-Yamato (U-Ym) tephra erupted from Ulleungdo (ca. 40 ka; SG14-3216), and the AT tephra (ca. 30 ka; SG06-2650) erupted from Aira (Albert et al., 2018, 2019; McLean et al., 2020; Smith et al., 2013). Since cryptotephra analysis is typically able to integrate eruption stratigraphies from more distal volcanic sources (e.g., Bourne et al., 2015; Cook et al., 2018; Jensen et al., 2014; Lane et al., 2015; Mackay et al., 2016; van der Bilt et al., 2017), it is possible that cryptotephra layers identified within these sediments may also originate from other more distal sources (>1,000 km)

**Table 1**  
Summary of the Tephra Layers Identified in the Sediments of the Lake Suigetsu (SG14 Core) Between 50 and 30 ka

Suigetsu Tephra Label	V / C	SG14 Master Core and Position	SG14 Composite Sampling Depth (cm)	Shards Per Gram	Glass Shard Morphology	Major Element Glass Compositions (wt. %)				Trace Element Analysis	Eruption Age (IntCal3 yrs BP; 95.4 % Confidence Interval)	Compositional Group (see text)	Source
						SiO <sub>2</sub>	K <sub>2</sub> O	CaO	n				
SG06-2650	V	G-6-base	2614.9	> 20,000	PL	77.02 - 78.41	3.24 - 3.55	1.03 - 1.20	35 <sup>1</sup>	19 <sup>2</sup>	30,174 - 29,982 <sup>2</sup>	3	AT, Aira <sup>1</sup>
SG14-2625	C	E-23 (6.0 - 7.0 cm)	2624.2 - 2625.2	9,838	MI, C, V	60.51 - 65.12	2.61 - 3.88	3.57 - 5.48	21	-	30,272 - 30,055	2	Aso
SG14-2649	C	E-23 (30.0 - 31.0 cm)	2648.2 - 2649.2	23,117	MI, PL	74.14 - 77.75	3.69 - 4.63	1.00 - 1.70	15	-	30,602 - 30,395	2	Aso
SG14-2706	C	F-28 (29.8 - 30.8 cm)	2705.4 - 2706.4	> 20,000	F, V	78.54 - 79.35	3.54 - 4.20	0.93 - 1.10	49	-	31,631 - 31,391	3	Ryukyu-Kyushu arc
SG14-2739	C	F-28 (62.8 - 63.8 cm)	2738.4 - 2739.4	8,367	PL, MI	63.70 - 65.18	3.58 - 3.92	3.39 - 4.20	16	-	32,380 - 32,111	2	Aso
SG14-2752	C	F-28 (75.8 - 76.8 cm)	2751.4 - 2752.4	10,067	F, C, MV	68.84 - 70.11	3.95 - 4.50	1.66 - 2.02	17	9	32,647 - 32,376	2	Aso
SG14-2814	C	F-29 (35.0 - 36.0 cm)	2813.3 - 2814.3	7,125	F	77.23 - 78.09	3.72 - 4.08	0.79 - 1.01	33	9	33,977 - 33,716	3	Aira
SG14-2830	C	E-30 (14.0 - 15.0 cm)	2828.6 - 2829.6	2,767	PL	73.91 - 75.80	2.70 - 2.94	1.43 - 2.49	16	8	34,368 - 34,111	3	Ryukyu-Kyushu arc
SG14-2838	C	E-30 (22.0 - 23.0 cm)	2836.6 - 2837.6	1,400	PU, MI	-	-	-	5	-	34,562 - 34,301	-	-
SG14-2841	C	E-30 (25.0 - 26.0 cm)	2839.6 - 2840.6	2,850	PL, MI	61.23 - 70.12	2.97 - 5.73	1.74 - 5.13	28	8	34,635 - 34,372	2	Aso
SG14-2856	C	E-30 (40.0 - 41.0 cm)	2854.6 - 2855.6	1,482	C, V	77.56 - 78.86	3.50 - 3.95	0.81 - 1.30	15	-	34,981 - 34,712	3	Aira
SG14-2873	C	E-30 (57.0 - 58.0 cm)	2871.6 - 2872.6	12,575	F, V	75.46 76.76	2.85 - 3.73	0.95 - 1.64	22	9	35,354 - 35,082	3	Aira
SG14-2941	C	E-31 (16.0 - 17.0 cm)	2939.6 - 2940.6	-	MI, P	-	-	-	-	-	36,633 - 36,329	-	-
SG14-2965	C	E-31 (40.0 - 41.0 cm)	2963.6 - 2964.6	1,950	V, MV, MI	74.14 - 74.65	0.74 - 0.81	2.56 - 2.80	4	-	37,085 - 36,755	4	Kurile arc
SG14-2995	C	E-31 (70.0 - 71.0 cm)	2993.6 - 2994.6	> 20,000	V	76.55 - 78.42	3.09 - 3.42	1.04 - 1.58	20	-	37,604 - 37,242	3	Ryukyu-Kyushu arc
SG14-3016	C	F-31 (24.0 - 25.0 cm)	3014.6 - 3015.6	6,567	PL, F	75.15 - 76.15	2.76 - 3.68	1.44 - 1.67	10	-	37,944 - 37,567	3	Ryukyu-Kyushu arc
SG14-3085	C	G-08 (52.0 - 53.0 cm)	3083.5 - 3084.5	4,400	PU	57.89 - 68.16	1.88 - 4.55	2.56 - 6.95	28	12	39,010 - 38,634	2	Aso
SG14-3216	V	G-09-06	3216.2	> 20,000	MV	59.46 - 62.92	5.79 - 7.23	1.14 - 1.55	37 <sup>4</sup>	9 <sup>4</sup>	40,332 - 39,816 <sup>4</sup>	1	U-Ym, Ulleungdo <sup>4</sup>
SG14-3336	C	F-34 (29.0 - 30.0 cm)	3335.1 - 3336.1	5,750	PU, MI	70.63 - 80.17	1.45 - 2.97	0.90 - 3.16	19	-	42,231 - 41,804	4	-
SG14-3380	C	E-35 (39.5 - 40.5 cm)	3378.9 - 3379.9	18,383	MV, F	65.45 - 67.95	5.31 - 5.67	0.85 - 1.56	16 <sup>4</sup>	10	42,750 - 42,323	1	B-Sg-42; Changbaishan
SG06-3485	V	E-36-04	3468.6	> 20,000	F, V, PL	53.11 - 55.43	0.33 - 0.67	8.50 - 10.58	13 <sup>1</sup>	13 <sup>2</sup>	44,013 - 43,413 <sup>2</sup>	-	Ko-Fuji <sup>2</sup>
SG14-3605	C	E-37 (58.3 - 59.3 cm)	3603.6 - 3604.6	2,200	MI, G	62.27 - 70.28	2.62 - 4.47	0.38 - 5.53	11	10	46,229 - 45,419	2	Aso
SG06-3668	V	E-37-13	3638.6	> 20,000	PU, MV, F	70.62 - 78.69	2.22 - 5.19	0.50 - 2.90	36 <sup>1,2</sup>	15 <sup>3</sup>	46,713 - 45,877 <sup>3</sup>	-	SI, Sambe <sup>3</sup>
SG14-3844	C	F-39 (25.0 - 26.0 cm)	3842.9 - 3843.9	16,013	F, V, MI	77.69 - 78.12	3.54 - 4.03	0.84 - 1.06	9	6	49,913 - 48,424	3	Aira
SG06-3912	V	F-39-07	3878.9	> 20,000	F, C	69.64 - 73.63	4.46 - 4.90	1.05 - 2.33	20 <sup>1,2</sup>	16 <sup>2</sup>	50,227 - 49,559 <sup>2</sup>	2	ACP4, Aso <sup>2</sup>

References: 1) Smith et al., 2013; 2) Albert et al. (2019); 3) Albert et al. (2018); 4) McLean et al. (2020); 5) This study. V / C = Visible / Cryptotephra layer, PU = Pumiceous, PL = Platy, C = Cuspate, F = Fluted, V = Vesicular, MV = Microvesicular, MI = Microtephra inclusions, G = Green, n = number of analyses. Tephra marked with a dash have not been able to be robustly correlated to a particular eruption or volcano. The sampling range is shown for cryptotephra layers and the base depth is shown for visible ash layers. The age of tephra SG06-3912 was extrapolated on the 'SG06-2012' chronology as reported in Albert et al. (2019).

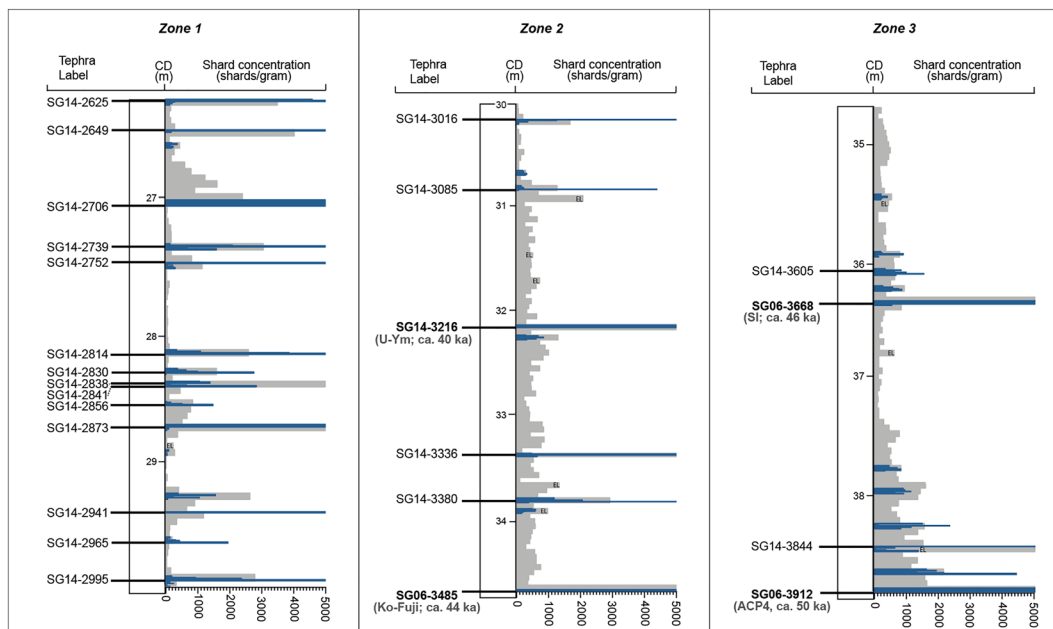


**Figure 2.** Glass shard concentrations (shards per gram of dry sediment; capped at 5,000) in the annually laminated sediments of the Lake Suigetsu SG14 core (50 to 30 ka). The tephrostratigraphy is divided into three zones (1–3) for illustrative purposes. Concentration of low-resolution (5 cm) samples are shown in gray, and high-resolution samples (1 cm) are overlain in blue. Tephra isochrons are labeled using their SG06/SG14 composite depth, with visible layers in bold. Peaks in shard concentrations that coincide with visible, high-energy event layers (EL) are not considered primary. SG06 visible tephra correlations and ages after Albert et al. (2018, 2019) and McLean et al. (2020).

across East Asia. For instance, ash erupted from the Izu-Bonin and NE Japan arc are preserved as low-concentration cryptotephra layers in the Holocene sediments of Lake Suigetsu (McLean et al., 2018).

### 3. Materials and Methods

#### 3.1. Cryptotephra Extraction Techniques

The master SG14 core (composite sequence) was contiguously subsampled at a ca. 5 cm resolution, from the ACP4 tephra (39.1 m CD) to the base of the AT tephra (26.5 m CD), avoiding the known high-energy event layers (e.g., flood horizons; Schlögl et al., 2014). If elevated peaks in shard concentrations were observed in the ca. 5 cm scan sample, the sediment was resampled at a 1 cm resolution to more precisely determine the stratigraphic positioning of the peak. All samples were wet sieved through a 25  $\mu\text{m}$  mesh and processed using the heavy liquid floatation method outlined by Turney (1998) and Blockley et al. (2005). The extraction residues were mounted on slides using Canada Balsam, and glass shards were counted via microscopic examination to quantify the number of shards per gram of dried sediment (s/g). Glass shards were extracted from samples chosen for geochemical analysis and hand-picked from a wetted-slide using a micromanipulator (see Lane et al., 2014). These shards were mounted in Epoxy resin stubs, which were sectioned and polished to expose a flat surface and carbon coated for electron microprobe analysis.

#### 3.2. Major Element Analysis of the Glass Shards

Major and minor element compositions of individual glass shards from the SG14 tephra layers and near-source reference material were measured using a JEOL-8600 wavelength-dispersive electron microprobe (WDS-EMP) at the Research Laboratory for Archaeology and History of Art (RLAHA), University of Oxford. Analyses used an accelerating voltage of 15 kV, beam current of 6 nA, and 10  $\mu\text{m}$ -diameter beam. Peak counting times were 12 s for Na, 50 s for Cl, 60 s for P, and for 30 s for all other elements. The electron microprobe was calibrated using a suite of mineral standards and the PAP absorption correction method was applied for quantification. The accuracy and precision of these data were assessed using analyses of the MPI-DING reference glasses (ATHO-G-1, StHs6/80-G, and GOR132-G) from the Max Planck Institute (Jochum et al., 2006), which were run as secondary standards. Analyses of these secondary standards lie



within two standard deviations centered on the preferred values and are presented in the supporting information. Data were filtered to remove non-glass analyses and those with analytical totals <93%. The raw values (given in the Supplementary Material) were normalized to 100% to better enable comparison and to account for variable hydration and are presented as such in all tables and figures in the main text.

### 3.3. Trace Element Analysis of the Glass Shards

Trace element compositions for the glass shards obtained from the SG14 sediments were measured by laser ablation inductively coupled plasma mass spectrometry (LA-ICP-MS) at the Department of Solid Earth Geochemistry, Japan Agency for Marine-Earth Science and Technology (JAMSTEC). The analytical equipment used include the deep-ultraviolet (200 nm) femtosecond laser ablation system (DUV-FsLA) of OK-Fs2000K (OK Laboratory, Tokyo, Japan) connected to the modified high-sensitivity sector field ICP-MS of Element XR (Thermo Scientific, Bremen, Germany). All analyses used a 25  $\mu\text{m}$  crater diameter and depth, and conditions followed those reported by Kimura and Chang (2012). Ten major elements including  $\text{P}_2\text{O}_5$  and 33 trace elements were analyzed for each sample and were also run alongside several MPI-DING reference glasses (Jochum et al., 2006) and the BHVO-2G standard provided by the Geological Survey of Japan. Accuracies of the BHVO-2G glass analyses are typically <3% for most elements, <5% for Sc, Ga, Sm, Eu, Gd, and U, and <10% for Ni, Cu, and Lu. Full trace element data sets and secondary standard analyses are provided in the supporting information.

Trace element compositions for proximal units Aso-Kpfa, A-Fm, and A-Kn were performed using an Agilent 8,900 triple quadrupole ICP-MS (ICP-QQQ) coupled to a Resonetics 193 nm ArF excimer laser-ablation system in the Department of Earth Sciences, Royal Holloway, University of London, using analytical procedures and data reduction (Microsoft Excel) methods outlined by Tomlinson et al. (2010). MPI-DING glasses (StHs6/80-G and ATHO-G-1; Jochum et al., 2006) were analyzed alongside the tephra deposits to monitor the accuracy. Full operating conditions used to analyze these reference samples are provided in the supporting information, along with the analyses of the MPI-DING glasses.

### 3.4. Chronology of the Lake Suigetsu Sediment Cores

A detailed Bayesian age model was used to determine the deposition age of ash layers identified in the Suigetsu sediments. The composite Suigetsu sedimentary sequence (correlation model ver. 08 May 2016) was modeled on to the IntCal13 timescale (Reimer et al., 2013) implementing three successive cross-referenced Poisson-process (“P\_Sequence”) depositional models using OxCal (ver. 4.3; Bronk Ramsey, 2008, 2017). These include 775 AMS  $^{14}\text{C}$  dates obtained from terrestrial plant macrofossils from the upper 38 m (SG06-CD) of the SG93 and SG06 cores (Kitagawa & van der Plicht, 1998a, 1998b, 2000; Staff et al., 2013a, 2013b) and varve counting between 12.88 and 31.67 m SG06 CD (Marshall et al., 2012; Schlolaut et al., 2012). SG06 Event Free Depths (EFDs; model ver. 29 Jan 2011) were used within the age model, which excludes instantaneous deposits >5 mm in thickness, (i.e., high-energy event layers, such as floods) (see Schlolaut et al., 2012; Staff et al., 2011).

## 4. Results

### 4.1. Tephrostratigraphy

Twenty-five ash layers (five visible and 20 cryptotephra layers) are identified in the SG14 varved sediments spanning 50 to 30 ka (39.1 m CD to 26.5 m CD) (Figure 2; Table 1). These ash layers are herein labeled using their SG14 composite depth in cm (SG14 correlation model 30 May 2017) that is rounded to the nearest integer (Table 1). For continuity, SG06 labels are used for the four visible tephra layers that were previously identified and geochemically characterized in the SG06 cores (Table 1; Figure 2).

Cryptotephra layers are clearly identified within the sediments as they are characterized by significant peaks in glass shard concentrations, which range from 1,400 to >20,000 s/g (Figure 2; Table 1). Glass shard characteristics (e.g., shard size, morphology, and color) vary considerably between isochrons (Table 1) but remain relatively uniform in each layer. This provides a first order discrimination between primary and secondary ash layers, since ash is well-sorted during dispersal, but reworking processes tend to mix glass from several sources (as observed in flood layers; McLean et al., 2018). On average, one ash layer per metre is observed between 39 and 30 m CD (Zones 3 and 2; Figure 2), whereas 15 ash layers are identified in the 4 m prior to the AT ash (30–26 m CD; Zone 1). Several of the cryptotephra identified in Zone 1 are

closely spaced; such as SG14-2841 and SG14-2838, which are only separated by 3 cm of sediment that is equivalent to ca. 50 years.

Despite the relatively high glass concentrations in primary isochrons, very low levels of background glasses (i.e., those identified consistently through the sediments) are observed, which indicates very little reworking of material in the lake catchment through this period. As expected, background glass concentrations are lowest in regions furthest from visible ash horizons, for example, throughout Zone 1 they remain below 100 s/g (Figure 2). Following (i.e., stratigraphically above) the 1 mm thick visible layer SG06-3912 (ACP4, Aso), similar shard characteristics and glass compositions are observed for ca. 1 m of sedimentation. Higher background concentrations are observed during the Holocene sediments (typically between 500 and 5,000 s/g), due to the presence of several much thicker visible ash layers at 10 ka and 7.3 ka (e.g., U-Oki and K-Ah tephra), which were more easily reworked and continuously in-washed from the local catchment (McLean et al., 2018).

#### 4.2. Glass Geochemical Compositions

Major and minor element glass compositions of the ash layers identified between 50 and 30 ka are presented in Table 2 and in Figure 3. The major element compositions of SG14-2941 and SG14-2838 could not be analyzed due to the high abundance of microlite inclusions within the glass. Trace element compositions were obtained for several cryptotephra layers with suitable shard sizes to further characterize and assist correlations (Table 2; Figure 4). The cryptotephra can be categorized using their glass affinities into four compositional groups, described below and outlined in Table 1.

Compositional Group 1 spans a wide  $\text{SiO}_2$  (58–72 wt.%) and  $\text{K}_2\text{O}$  (2–5 wt.%) range and include seven cryptotephra layers and one visible (SG06-3912) tephra layer (Table 1). Four of these tephra layers have homogeneous compositions (SG14-2625, SG14-2649, SG14-2739, and SG14-2752), and three are heterogeneous (SG14-2841, SG14-3085, and SG14-3605) with both silicic (population a) and less evolved (population b) end-members (Figures 4a and 4b). When normalized to the primitive mantle (Sun & McDonough, 1989), the lower  $\text{SiO}_2$  population glasses are less enriched in Large Ion Lithophile Elements (LILE; e.g., Rb, Ba, and K) and High Field Strength Elements (HFSE), compared to the silicic population, and possess very similar Rare Earth Element (REE) profiles with light REE enrichment relative to the heavy REEs (La/Yb ratio). Compositional Group 1 shows strong depletions in Nb and Ta (Figure 4) consistent with subduction related genesis.

Compositional Group 2 is characterized by highly silicic glass compositions ( $>75$  wt.%  $\text{SiO}_2$ ), which all have  $>2.7$  wt.%  $\text{K}_2\text{O}$  (Figure 3). Four of these tephra layers contain glasses that are very homogenous and compositionally similar (SG14-3814, SG14-2856, SG14-2873, and SG14-3844), which are also distinguished by their low CaO (0.79–1.64 wt.%) content. Furthermore, SG14-2814, SG14-2873, and SG14-3844 all have identical mantle normalized profiles, which can be easily distinguished from Compositional Group 1 by more pronounced Eu anomalies and steeper REE profiles (La/Yb; Table 2; Figure 4). This subgroup is also less enriched in HFSE, in particular Nb (Figures 4c and 4d). In comparison, silicic glasses from SG14-2830 have similar mantle normalized profiles, but lower in light REE, and therefore exhibit a flatter REE profile (La/Yb ratios).

Compositional Group 3 consists of tephra layers SG14-3336 and SG14-2965, which contain medium and low-K glasses, respectively. SG14-3336 glass compositions are particularly heterogeneous, with  $\text{SiO}_2$  from 70.5 to 80.0 wt.%,  $\text{K}_2\text{O}$  from 1.45 to 2.97, and CaO from 0.90 to 3.16 wt.% (Figure 3). The four geochemical analyses for SG14-2965 (and several other low-total results; supporting information) show that these are very distinctive from the other SG14 glasses presented here, with  $\text{SiO}_2$  from 74.14 to 74.65 wt.%,  $\text{K}_2\text{O}$  from 0.74 to 0.81 wt.%, and CaO from 2.56 to 2.80 wt.%. Unfortunately, trace element compositions could not be determined for SG14-3336 and SG14-2965 as the shape and size of the shards meant that there was not sufficient area for analysis.

Compositional Group 4 comprises two alkali-rich ( $\text{Na}_2\text{O} + \text{K}_2\text{O} \geq 10$  wt. %) tephra layers, named SG14-3380 and the visible deposit SG14-3216, which are classified as phonolites and trachytes, respectively (Figure 3c). When normalized to the primitive mantle (Sun & McDonough, 1989), both tephra show significant depletions in Ba, Sr, and Eu, typical of K-feldspar fractionation (Figures 4e and 4f). SG14-3216 has a Y/Th ratio of

**Table 2**  
Major and Trace Element Glass Compositions (Normalized) of the Newly Identified Ash Layers Preserved in the SG14 Core Between 50 and 30 ka ( $\text{FeO}^T = \text{All Fe Reported as FeO}$ ). Raw Data Sets and Secondary Standards are Included in the Supporting Information. Major and Trace Element Data for SG14-3380 and SG14-3216 Are From McLean et al. (2020).

	SG14-2625		SG14-2649		SG14-2706		SG14-2739		SG14-2752		SG14-2814		SG14-2830		SG14-2841a		SG14-2841b		SG14-2856		SG14-2873		SG14-2965	
wt. (%)	Avg.	$\pm 1\sigma$	Avg.	$\pm 1\sigma$	Avg.	$\pm 1\sigma$	Avg.	$\pm 1\sigma$	Avg.	$\pm 1\sigma$	Avg.	$\pm 1\sigma$	Avg.	$\pm 1\sigma$	Avg.	$\pm 1\sigma$	Avg.	$\pm 1\sigma$	Avg.	$\pm 1\sigma$	Avg.	$\pm 1\sigma$	Avg.	$\pm 1\sigma$
$\text{SiO}_2$	61.78	1.05	74.72	0.87	78.97	0.16	64.41	0.36	69.54	0.32	77.76	0.19	75.27	0.46	68.10	1.35	61.95	0.40	77.95	0.20	77.87	0.62	74.32	0.20
$\text{TiO}_2$	1.21	0.11	0.41	0.07	0.13	0.03	0.97	0.04	0.74	0.05	0.11	0.03	0.59	0.04	0.84	0.07	1.11	0.03	0.11	0.03	0.14	0.05	0.23	0.03
$\text{Al}_2\text{O}_3$	15.56	0.30	13.25	0.30	12.40	0.10	15.45	0.13	15.24	0.22	12.49	0.09	12.51	0.32	15.11	0.62	16.20	0.01	12.34	0.16	12.60	0.34	13.34	0.10
$\text{FeO}^T$	6.95	0.57	1.73	0.21	1.13	0.08	5.34	0.21	2.67	0.12	1.04	0.07	2.26	0.12	3.58	0.42	6.20	0.53	1.05	0.11	1.06	0.16	3.31	0.21
MnO	0.15	0.07	0.04	0.03	0.05	0.04	0.09	0.05	0.12	0.04	0.04	0.02	0.05	0.03	0.11	0.05	0.15	0.01	0.05	0.04	0.04	0.03	0.16	0.06
MgO	2.11	0.22	0.35	0.08	0.12	0.02	1.56	0.08	0.62	0.06	0.10	0.03	0.43	0.06	0.88	0.23	2.15	0.10	0.13	0.03	0.13	0.04	0.25	0.03
CaO	4.90	0.42	1.59	0.17	1.03	0.04	3.70	0.19	1.85	0.10	0.90	0.06	1.83	0.21	2.47	0.54	5.06	0.01	1.06	0.11	1.07	0.14	2.69	0.09
$\text{Na}_2\text{O}$	3.91	0.16	3.44	0.14	3.60	0.14	4.34	0.13	4.64	0.16	3.54	0.13	4.04	0.10	4.20	0.24	3.70	0.22	3.59	0.11	3.36	0.16	4.61	0.14
$\text{K}_2\text{O}$	3.04	0.27	4.42	0.22	3.69	0.10	3.73	0.10	4.29	0.14	3.89	0.08	2.81	0.08	4.49	0.42	3.03	0.01	3.70	0.14	3.57	0.18	0.78	0.03
$\text{P}_2\text{O}_5$	0.41	0.02	0.04	0.02	0.02	0.02	0.41	0.04	0.13	0.02	0.02	0.02	0.09	0.02	0.19	0.06	0.36	0.04	0.02	0.02	0.03	0.02	0.06	0.01
Cl	-	-	-	-	-	-	-	-	0.14	0.03	0.12	0.01	0.11	0.02	0.11	0.01	0.08	0.01	-	-	0.12	0.03	0.25	0.04
<i>n</i>	21	15	15	49	17	33	16	-	17	16	33	16	16	26	26	2	2	15	15	22	22	5	5	5
<b>ppm</b>																								
Rb	-	-	-	-	-	-	-	-	131.84	6.28	153.31	10.16	82.56	2.97	133.45	28.86	85.47	-	-	-	144.54	7.06	-	-
Sr	-	-	-	-	-	-	-	-	175.86	17.17	54.79	6.53	101.52	2.55	225.17	106.11	325.70	-	-	-	62.68	4.05	-	-
Y	-	-	-	-	-	-	-	-	34.69	2.40	23.75	2.21	37.16	1.26	37.04	3.62	31.15	-	-	-	21.77	1.56	-	-
Zr	-	-	-	-	-	-	-	-	260.52	12.63	92.34	7.03	205.41	7.77	272.92	43.04	195.62	-	-	-	96.33	3.54	-	-
Nb	-	-	-	-	-	-	-	-	15.89	0.87	7.48	0.92	6.49	0.68	17.01	2.80	11.36	-	-	-	7.48	0.83	-	-
Ba	-	-	-	-	-	-	-	-	623.29	23.55	568.58	56.15	387.48	14.19	648.38	57.94	480.77	-	-	-	523.60	22.10	-	-
La	-	-	-	-	-	-	-	-	27.57	1.69	25.46	2.54	17.33	0.96	29.83	4.00	23.04	-	-	-	24.04	1.45	-	-
Ce	-	-	-	-	-	-	-	-	62.48	3.19	51.23	5.00	39.18	2.18	67.14	8.71	52.20	-	-	-	48.17	2.30	-	-
Pr	-	-	-	-	-	-	-	-	7.36	0.52	5.18	0.64	4.71	0.37	7.98	1.08	6.21	-	-	-	4.81	0.40	-	-
Nd	-	-	-	-	-	-	-	-	29.94	2.30	18.61	2.58	19.96	0.69	32.04	5.39	25.04	-	-	-	17.70	3.68	-	-
Sm	-	-	-	-	-	-	-	-	6.85	0.79	3.96	1.56	4.44	0.45	6.71	2.13	7.29	-	-	-	3.78	1.24	-	-
Eu	-	-	-	-	-	-	-	-	1.30	0.16	0.55	0.29	1.11	0.29	1.24	0.27	1.99	-	-	-	0.37	0.27	-	-
Gd	-	-	-	-	-	-	-	-	5.60	1.62	2.54	2.75	4.20	1.42	7.54	2.06	5.46	-	-	-	2.64	2.01	-	-
Dy	-	-	-	-	-	-	-	-	5.51	0.83	3.62	0.73	5.54	0.87	5.54	1.50	3.97	-	-	-	2.95	0.60	-	-
Er	-	-	-	-	-	-	-	-	3.29	0.66	2.07	0.63	3.49	0.48	3.83	0.87	2.46	-	-	-	2.03	0.45	-	-
Yb	-	-	-	-	-	-	-	-	3.69	0.41	2.79	0.93	3.67	0.80	4.33	0.90	2.94	-	-	-	2.40	0.78	-	-
Hf	-	-	-	-	-	-	-	-	6.56	0.68	3.34	0.61	5.70	0.49	7.25	1.47	4.14	-	-	-	3.40	0.66	-	-
Ta	-	-	-	-	-	-	-	-	1.04	0.21	0.77	0.13	0.53	0.09	1.17	0.31	0.86	-	-	-	0.67	0.17	-	-
Th	-	-	-	-	-	-	-	-	12.30	0.68	15.15	1.44	7.76	0.65	13.47	2.47	8.88	-	-	-	14.28	0.61	-	-
U	-	-	-	-	-	-	-	-	3.27	0.15	3.26	0.36	1.83	0.16	3.47	0.82	2.16	-	-	-	2.94	0.48	-	-
Y/Th	-	-	-	-	-	-	-	-	2.82	0.20	1.58	0.17	4.81	0.35	2.79	0.30	3.51	-	-	-	1.53	0.13	-	-
Zr/Th	-	-	-	-	-	-	-	-	21.20	0.85	6.12	0.48	26.57	1.83	20.36	1.24	22.02	-	-	-	6.76	0.38	-	-
<i>n</i>	-	-	-	-	-	-	-	-	9	9	9	9	8	8	7	1	1	9	9	9	9	9	9	9



**Table 2**  
Continued

wt. (%)	SG14-2995		SG14-3016		SG14-3085a		SG14-3085b		SG14-3216		SG14-3336		SG14-3380		SG14-3486		SG14-3605a		SG14-3605b		SG14-3844	
	Avg.	±1σ	Avg.	±1σ	Avg.	±1σ	Avg.	±1σ	Avg.	±1σ	Avg.	±1σ	Avg.	±1σ	Avg.	±1σ	Avg.	±1σ	Avg.	±1σ	Avg.	±1σ
SiO <sub>2</sub>	77.36	0.61	75.96	0.14	67.68	0.68	59.34	1.15	60.75	0.67	76.97	2.56	66.26	0.70	53.83	0.63	70.18	0.15	64.51	1.86	77.90	0.16
TiO <sub>2</sub>	0.35	0.04	0.57	0.04	0.88	0.30	1.04	0.07	0.39	0.07	0.18	0.06	0.60	0.09	1.32	0.19	0.82	0.03	1.16	0.12	0.10	0.03
Al <sub>2</sub> O <sub>3</sub>	12.14	0.24	12.15	0.17	14.44	0.31	16.00	0.74	19.85	0.28	13.01	1.34	14.97	0.28	17.01	1.49	13.86	0.09	15.58	0.77	12.27	0.11
FeO <sup>1</sup>	1.47	0.16	2.16	0.14	4.39	0.29	7.84	0.70	3.12	0.16	1.29	0.71	5.12	0.14	0.48	0.09	3.68	0.17	5.21	0.57	0.85	0.09
MnO	0.05	0.03	0.10	0.04	0.10	0.04	0.17	0.03	0.18	0.05	0.08	0.05	0.15	0.04	0.17	0.07	0.10	0.01	0.11	0.04	0.04	0.03
MgO	0.27	0.05	0.41	0.04	1.00	0.07	2.78	0.63	0.17	0.07	0.73	0.82	0.25	0.06	4.73	0.76	0.96	0.02	1.54	0.33	0.10	0.02
CaO	1.34	0.15	1.60	0.09	2.89	0.40	6.23	0.63	1.34	0.12	1.79	0.70	1.24	0.17	9.37	0.50	2.44	0.08	4.23	0.77	0.91	0.08
Na <sub>2</sub> O	3.70	0.15	3.95	0.16	3.88	0.19	3.62	0.31	7.28	0.96	3.44	0.54	5.67	0.66	2.69	0.24	3.23	0.17	3.88	0.19	3.83	0.09
K <sub>2</sub> O	3.31	0.07	3.04	0.32	4.39	0.12	2.63	0.38	6.50	0.33	2.33	0.42	5.49	0.09	0.48	0.09	4.47	0.01	3.35	0.41	3.87	0.19
P <sub>2</sub> O <sub>5</sub>	0.02	0.01	0.07	0.03	0.26	0.03	0.29	0.05	0.05	0.03	0.07	0.03	0.09	0.03	0.20	0.03	0.31	0.07	0.31	0.07	0.02	0.02
Cl	-	-	-	-	0.09	0.01	0.07	0.02	0.37	0.10	0.10	0.03	0.16	0.02	0.07	0.02	0.13	0.03	0.13	0.03	0.10	0.01
n	20	-	6	-	5	-	23	-	37	19	14	13	14	13	-	2	9	9	9	9	9	9
ppm																						
Rb	-	-	-	-	142.34	4.71	74.48	8.48	195.42	19.06	-	-	143.55	8.91	-	-	123.00	25.59	88.93	3.68	146.33	11.47
Sr	-	-	-	-	211.75	21.88	409.30	70.34	14.31	10.20	-	-	25.01	24.41	-	-	273.84	99.60	351.22	31.88	52.25	7.96
Y	-	-	-	-	40.21	3.03	30.52	3.18	26.04	2.94	-	-	51.11	3.94	-	-	30.10	5.46	32.64	2.49	18.19	2.52
Zr	-	-	-	-	297.08	8.27	167.36	18.16	709.63	104.31	-	-	741.36	45.81	-	-	267.43	78.60	268.35	14.59	74.00	14.87
Nb	-	-	-	-	17.54	1.58	10.08	0.89	175.17	21.16	-	-	96.98	5.52	-	-	13.67	1.58	12.65	0.82	7.11	0.54
Ba	-	-	-	-	663.24	35.11	464.95	23.96	16.29	13.34	-	-	77.31	57.26	-	-	695.85	75.80	649.66	20.93	508.70	28.90
La	-	-	-	-	33.09	2.34	20.80	2.65	98.17	9.04	-	-	76.42	4.75	-	-	34.25	2.72	32.95	0.47	21.73	1.19
Ce	-	-	-	-	71.68	2.18	48.11	4.20	161.66	15.70	-	-	154.34	9.55	-	-	71.11	6.93	68.96	5.34	43.75	2.77
Pr	-	-	-	-	8.99	0.22	6.14	0.83	14.46	1.24	-	-	17.05	1.14	-	-	8.14	0.94	8.23	0.35	4.56	0.52
Nd	-	-	-	-	39.35	2.52	26.13	3.30	43.92	4.69	-	-	65.57	6.37	-	-	33.59	5.09	33.51	3.63	15.62	1.57
Sm	-	-	-	-	8.55	0.60	6.13	1.12	6.41	0.70	-	-	12.91	1.91	-	-	5.91	2.74	6.96	0.43	3.22	0.88
Eu	-	-	-	-	1.75	0.20	1.38	0.36	0.59	0.24	-	-	0.61	0.20	-	-	1.58	0.36	1.81	0.18	0.41	0.11
Gd	-	-	-	-	6.97	0.61	5.31	1.96	5.45	1.93	-	-	10.69	1.42	-	-	7.36	1.12	6.97	2.07	3.01	1.89
Dy	-	-	-	-	6.21	1.99	5.39	1.18	4.44	0.61	-	-	9.26	0.89	-	-	5.83	1.28	5.54	1.28	2.88	0.31
Er	-	-	-	-	4.38	0.32	3.07	0.69	2.77	0.62	-	-	5.08	0.73	-	-	2.61	0.75	3.41	1.10	2.23	0.25
Yb	-	-	-	-	3.96	0.38	2.75	0.77	3.09	0.70	-	-	4.30	0.59	-	-	3.11	0.83	3.71	0.54	1.78	0.23
Hf	-	-	-	-	8.36	0.74	4.16	0.54	13.39	2.09	-	-	16.92	1.24	-	-	6.80	1.97	6.40	0.74	2.45	0.58
Ta	-	-	-	-	1.40	0.29	0.59	0.20	9.72	1.09	-	-	5.56	0.46	-	-	0.79	0.16	0.64	0.31	0.77	0.22
Th	-	-	-	-	15.00	1.78	7.21	0.71	25.23	3.23	-	-	14.14	1.05	-	-	12.17	2.75	9.49	0.88	13.63	1.07
U	-	-	-	-	3.70	0.12	1.82	0.29	5.29	0.86	-	-	2.79	0.34	-	-	2.21	0.46	1.64	0.16	2.86	0.21
Y/Th	-	-	-	-	2.69	0.15	4.24	0.31	1.04	0.07	-	-	3.62	0.23	-	-	2.59	0.69	3.45	0.26	1.35	0.26
Zr/Th	-	-	-	-	19.96	1.94	23.25	1.70	28.14	2.30	-	-	52.56	3.32	-	-	23.48	8.80	28.39	1.67	5.50	1.41
n	-	-	-	-	3	-	9	-	8	10	-	-	5	5	-	-	5	5	5	5	6	6

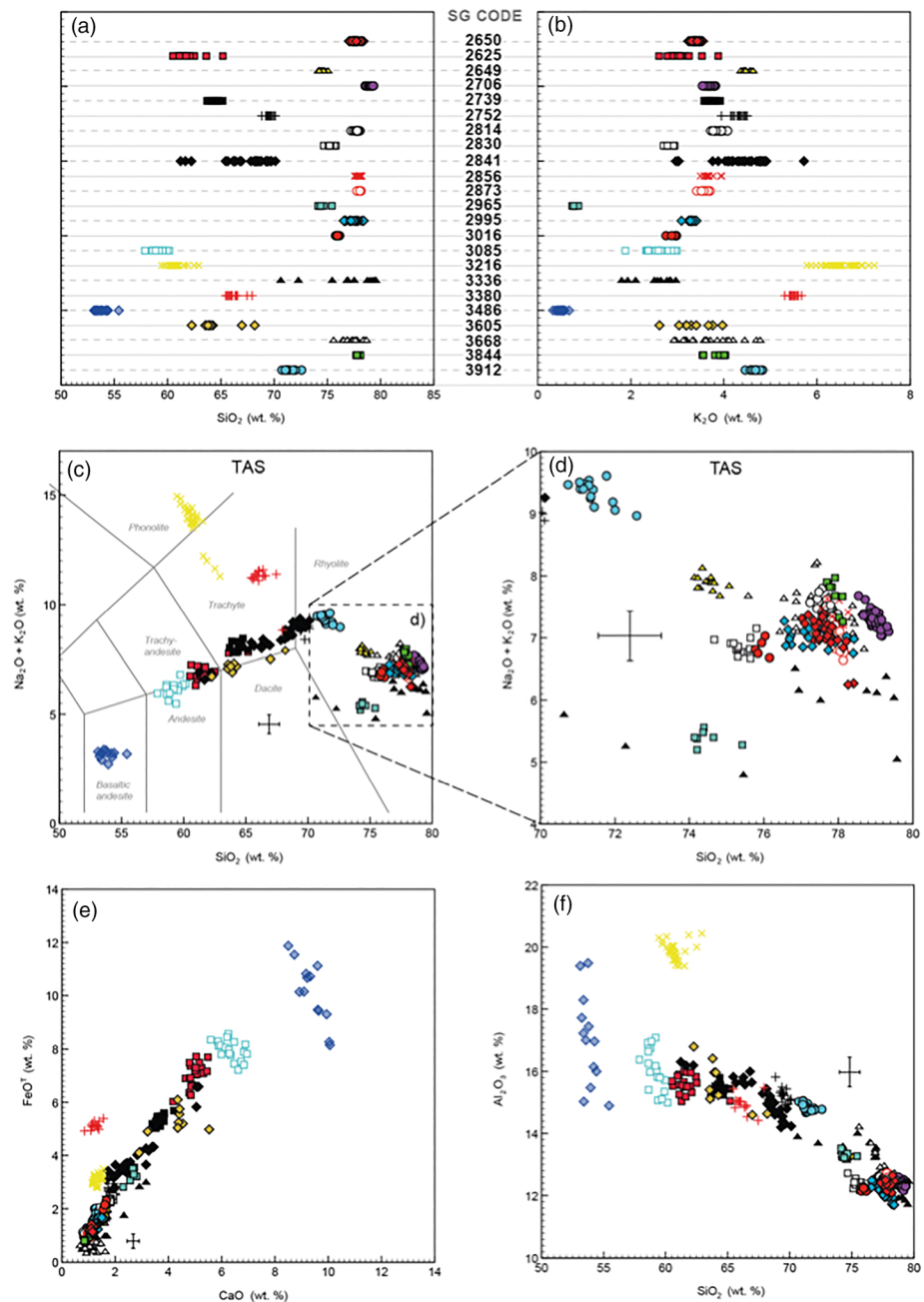


**Figure 3.** Major element compositions of the tephra layers preserved within the laminated sediments of Lake Suigetsu (SG14 core) between 50 and 30 ka. These are labeled using their SG06/SG14 composite depths. (a, b) SiO<sub>2</sub> and K<sub>2</sub>O compositions of tephra layers versus their stratigraphic position. (c, d) Total alkalis versus silica plot (TAS; with whole-rock classification based on Le Bas et al., 1986). (e, f) Bivariate plots for FeO<sup>T</sup>, CaO, SiO<sub>2</sub>, and Al<sub>2</sub>O<sub>3</sub> (error bars represent  $2 \times$  standard deviation of repeat analyses of the StHs6/80-G MPI-DING standard glass).

$1.04 \pm 0.70$ , whereas for SG14-3380, it is  $3.62 \pm 0.23$  (Table 2). The paucity of depletions in Nb and Ta within these volcanic glasses is inconsistent with subduction related volcanism (e.g., Kimura et al., 2015; Figure 4).

## 5. Provenance of the Suigetsu Cryptotephra Identified Between 50 and 30 ka

### 5.1. Geochemically Discriminating Volcanic Sources

Geochemical glass data sets for key widespread ash layers in East Asia are well established (e.g., Albert et al., 2019, and references therein; Kimura et al., 2015; Machida & Arai, 2003; McLean et al., 2018;

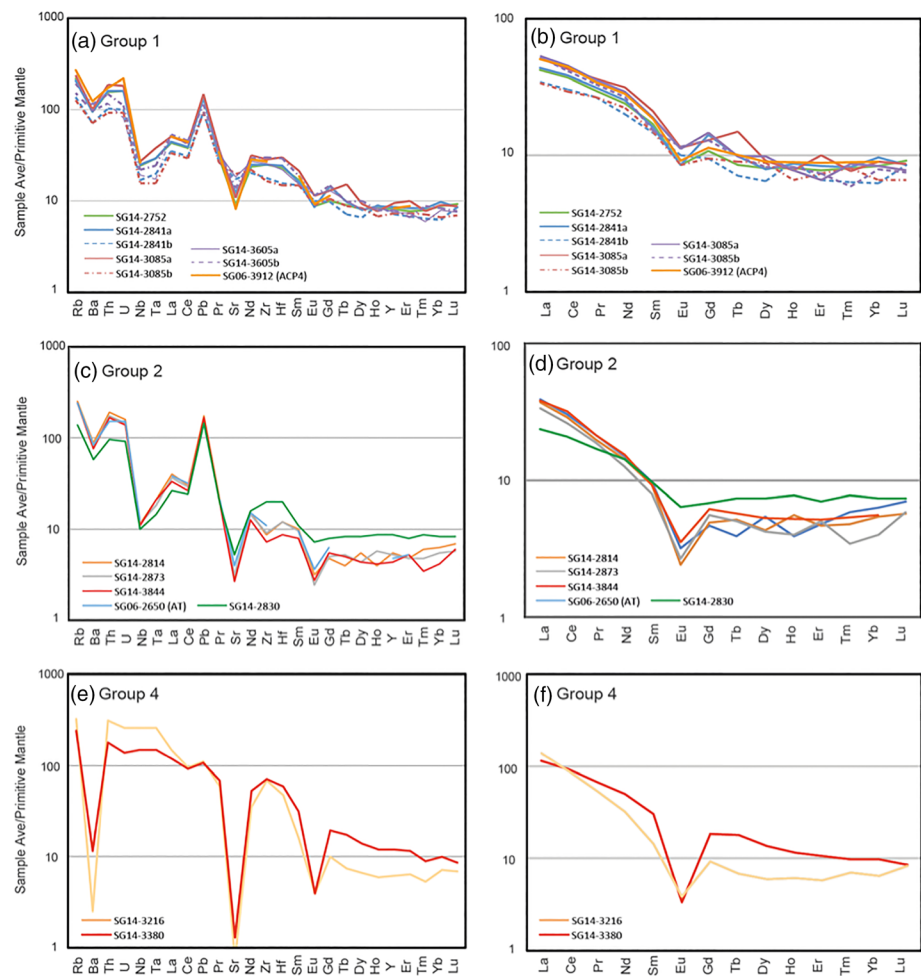


**Figure 4.** Average primitive mantle normalized glass compositions [of Sun & McDonough, 1989] of the tephra layers (compositional groups 1, 2, and 4) preserved within the laminated sediments of Lake Suigetsu (SG14 core) between 50 and 30 ka. Trace element data for SG06-3912 (ACP4) and SG06-2650 (AT) are from Albert et al. (2019), and SG14-3216 and SG14-3380 are from McLean et al. (2020).

Nakamura, 2016; Okuno et al., 2011; Schindlebeck et al., 2018), and their characteristics can be used to help provenance the tephra layers preserved in the Lake Suigetsu sequence.

It is relatively straightforward to distinguish tephra erupted from different arc sources distributed along the length of Japan, which can typically be discriminated by their  $\text{SiO}_2$  to  $\text{K}_2\text{O}$  ratios (Figures 5a and 5b). For instance, Late Quaternary glasses erupted from the Kyushu Central Volcanic Region (CVR; e.g., Aso) and Southern Volcanic Region (SVR; e.g., Aira, Ata, and Kikai) typically contain medium to high-K compositions and are clearly distinguishable at a major element level from tephra deposits erupted at volcanoes along the SW and NE Japan arcs (see Albert et al., 2019; Kimura et al., 2015; Figure 5). Vitreous tephra deposits erupted from Aso have the highest known  $\text{K}_2\text{O}$  content produced at a Japanese volcano ( $>3$  wt.%  $\text{K}_2\text{O}$  at 66 wt.%  $\text{SiO}_2$ ), and the most evolved ( $\sim 70$ –72 wt.%  $\text{SiO}_2$ ) extend to 6 wt.%  $\text{K}_2\text{O}$ ) and are therefore some of the most compositionally distinct. However, some centres (e.g., Kikai, Ata and Aira) erupt very compositionally similar tephra over tens to hundreds of thousands of years, with only slight major element variances. Therefore, trace element compositions, which reflect more subtle source characteristics and magmatic processes (e.g., Allan et al., 2008; Tomlinson et al., 2010), can be used to successfully fingerprint these sources. Vitreous tephra derived from all sources in Japan are enriched in LILE (e.g., Rb, Ba, and K) relative to REE (e.g., La to Yb) (Albert et al., 2019; Kimura et al., 2015), which is expected given their subduction genesis. Since, LILE concentrations are linked to  $\text{K}_2\text{O}$ , these elements are also very useful discriminators between

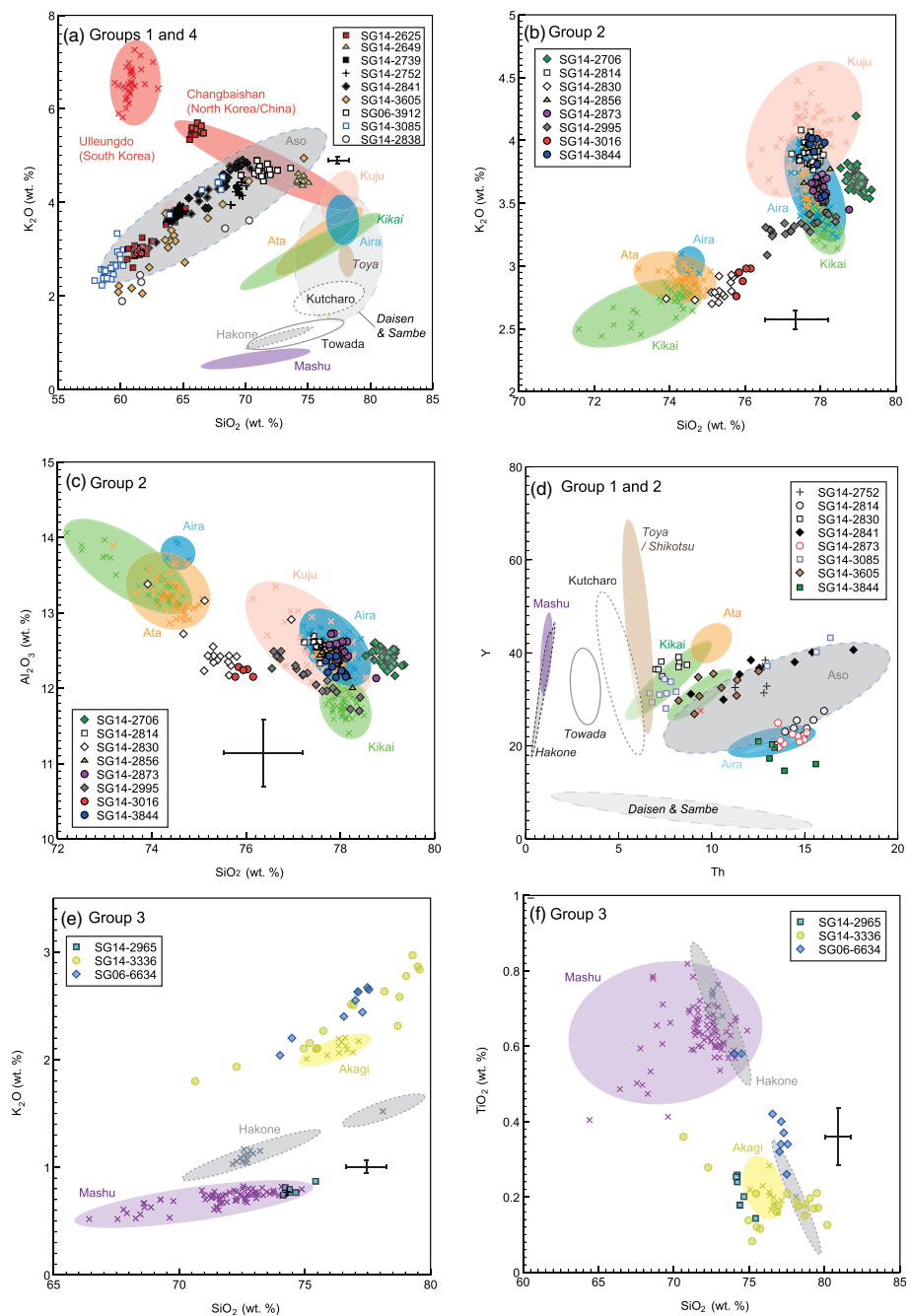


**Figure 5.** Major and trace element compositions of the SG14 cryptotephra layers (50 to 30 ka) in comparison to those established for major eruptive centers in East Asia. Proximal geochemical fields are shown for Japanese volcanoes (data from Albert et al., 2019), Changbaishan volcano (North Korea/China; Chen et al., 2016; McLean et al., 2016, 2020), and Ulleungdo volcano (South Korea; McLean et al., 2018, 2020; Smith et al., 2011). Error bars represent  $2 \times$  standard deviation of repeat analyses of the StHs6/80-G MPI-DING standard glass.

different arc sources (Figures 5d–5f). Furthermore, Y and Th can clearly separate glass erupted from the Kyushu calderas situated in the fore-arc (e.g., Kikai, Aira and Aira) (Albert et al., 2019; Figure 5d). Only intraplate volcanoes Ulleungdo (South Korea) and Changbaishan (North Korea/China) are known to have dispersed alkaline tephra across Japan during the Quaternary (Chen et al., 2019; Lim et al., 2013; Machida & Arai, 2003; McLean et al., 2020; Sun et al., 2014) and are therefore easily discriminated from those originating from Japan and other nearby arc settings.

In summary, the SG14 cryptotephra layers identified are provenanced to the following source regions or volcanoes.

1. **Group 1** : Kyushu Central Volcanic Region (CVR), Japan: Aso caldera, ( $n = 8$  layers preserved in Lake Suigetsu between 50 and 30 ka).
2. **Group 2**: Kyushu Southern Volcanic Region (SVR), Japan: Aira, and other southern Kyushu sources ( $n = 3$ ).
3. **Group 3**: Central and northern Honshu/Kurile arc tephtras, ( $n = 2$ ).
4. **Group 4**: Ulleungdo (South Korea) and Changbaishan (North Korea/China), ( $n = 2$ ).

These correlations and groups are discussed in detail below, as well as other tephtras that have not been correlated to known eruptions or volcanoes. Group 4 tephtras that are derived from intraplate volcanic sources west of the Japanese arc (e.g., SG14-3216 and SG14-3380) are comprehensively reviewed by McLean et al. (2020), in order to place these eruptions within the known eruptive records of Changbaishan and Ulleungdo volcanoes.

## 5.2. Group 1: Aso Caldera, Kyushu CVR (Japan)

Aso caldera (32°53'04"N, 131°06'14"E) is situated 530 km SW from Lake Suigetsu on the Kyushu CVR arc (Figure 1). Aso is one of the largest active volcanoes on Earth, and the caldera was formed by a series of at least four VEI 6–7 eruptions (oldest to youngest; Newhall and Self, ): Aso-1 (ca. 270 ka), Aso-2 (ca. 140 ka), Aso-3 (ca. 112–134 ka), and Aso-4 (ca. 86–87 ka; correlated to SG06-4963 in Lake Suigetsu; Aoki, (2008); Albert et al. (2019)). Post-caldera cones that formed after the Aso-4 eruption cycle are thought to have produced small, frequent explosive episodes that have generated deposits over 100 m thick on the eastern side of the caldera (Miyabuchi, 2009). The largest magnitude post-Aso-4 eruptions are associated with the Aso Central Cone (Miyabuchi, 2009), the most significant of which producing the Aso Central Cone Pumice 4 (ACP4; VEI 4; Takada, 1989) tephra deposit, which is correlated to tephra SG06-3912 (50.3 ka; Albert et al., 2019). This ash layer marks the basal depth of the cryptotephra investigations presented here.

Miyabuchi (2009, 2011) provides details of proximal evidence of other post-caldera forming events that occurred between the deposition of the ACP4 (ca. 50 ka; SG06-3912) and AT ash (ca. 30 ka) (summarized in Figure 6a). Notably, a period of intense silicic, explosive activity is estimated to have occurred between 31 and 30 ka, directly following the formation of a thick soil and prior to the AT eruption (Miyabuchi, 2009, 2011; Figure 6a). This activity includes the Aso-Kusasenrigahama pumice (Kpfa; Watanabe et al., 1982), which is found 1 m below the AT ash in the proximal stratigraphy and is thought to be the most voluminous of the fall units erupted from the Kusasenrigahama crater (2.21 km<sup>3</sup> bulk volume; Miyabuchi, 2011). Proximally, the Aso-Kpfa is characterized by six fall units at outcrops to the east of the caldera (E1–E6) and five units to the west (W1–W5) (Miyabuchi et al., 2003, 2004), implying numerous eruptive phases and a fluctuating dispersal axis (Miyabuchi, 2009).

As outlined above, glass compositions from Aso are easily discriminated from other centers across Japan and, importantly, those situated further south in the Kyushu SVR (e.g., Aira, Kikai, Ata) (Figure 5a), due to their clear HKCA affinity. Characteristically, glass erupted from Aso has a wide compositional range, from basalt to rhyolite (Figures 5c and 5d), which has been sequentially erupted during caldera forming events (e.g., Aso-3 eruption; Kaneko et al., 2015). Whole rock data of the proximal units identified by Miyabuchi (2009, 2011) between 67 and 30 ka suggest that explosive mafic (basaltic to basaltic andesitic; SiO<sub>2</sub> = 48–56 wt.%) eruptions were dominant, with infrequent silicic pumice and ash fall events (e.g., Aso-Kpfa; Ono, 1989; Miyabuchi, 2009). Detailed proximal volcanic glass data sets derived from the eruptive products of Aso during the 50 to 30 ka timeframe are not yet available, apart from the Aso-Kpfa deposit, which is characterized within this study. We find the Aso-Kpfa glass compositions are exclusively rhyolitic, containing ca. 69.5 wt.% SiO<sub>2</sub> 4.3 wt.% K<sub>2</sub>O (Figures 6c–6e). Trace element glass compositions are also typical of those erupted from Aso and are relatively homogeneous (e.g., Th = 11.9 ± 1.6 ppm; Y = 33.8 ± 4.5 ppm [2.s.d]) compared to the other characterized Aso units (Figure 6f).

Seven cryptotephra layers identified in the Lake Suigetsu sediments (SG14-2625, SG14-2649, SG14-2739, SG14-2752, SG14-2841, SG14-2997, SG14-3085) have HKCA glass compositions and are characteristic of



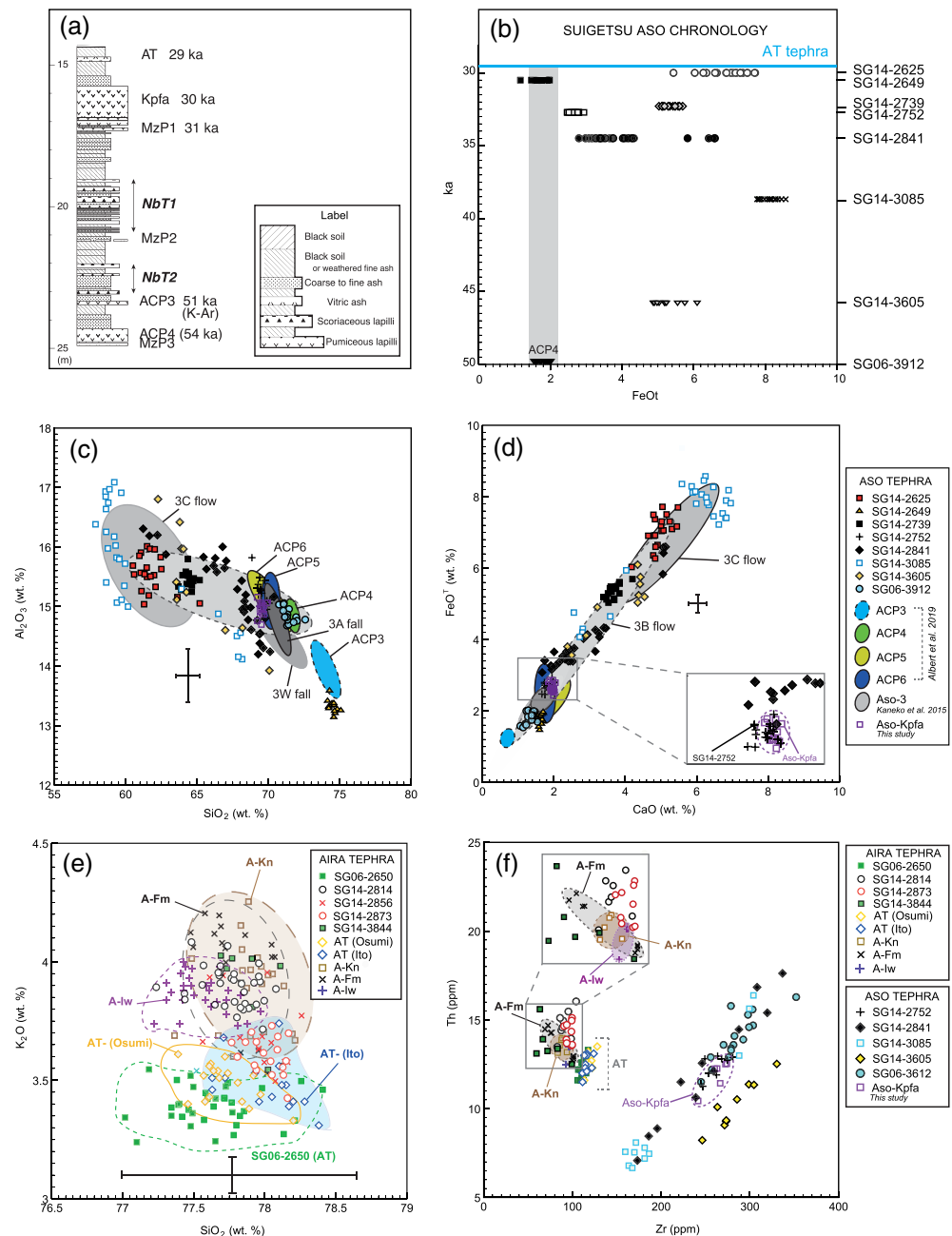


**Figure 6.** (a) Proximal volcanic stratigraphy compiled at outcrops at Aso caldera (Miyabuchi, 2011), (b)  $FeO^T$  content versus Suigetsu age for Aso derived tephra layers, (c, d) major element glass compositions of compositional Group 2 (Aso derived tephra layers) in comparison to other proximal deposits derived from Aso outcrops (Albert et al., 2019) including fields (in gray) for glass compositions of the Aso-3 (3W, 3C, and 3A) event (Kaneko et al., 2015), (e, f) major and trace element compositions for Aira derived tephras (compositional Group 3) in relation to Aira proximal glass chemistries (Albert et al., 2019; Smith et al., 2013; this study).

those derived from Aso (Figures 6b–6d). These glasses range from mafic (e.g., SG14-2625), intermediate (e.g., SG14-2841), and silicic (e.g., SG14-2649, SG14-2649) in composition, or in the case of SG14-3085 and SG14-3605, the glasses span the entire compositional range. Trace element signatures of SG14-2752, SG14-2841, SG14-3085, and SG14-3605 are enriched in the LILE (Rb) and HFSE (Th, U, Zr), typical of Aso glasses (Figure 4a). Due to the lack of detailed proximal volcanic glass data sets it is not yet possible to correlate the majority of the identified SG14 cryptotephra to specific units identified in the near source

realm. However, here we are able to show that only the glasses of SG14-2752 geochemically overlap those of the newly analyzed Aso-Kpfa proximal deposit (Figures 6c, 6d, and 6f).

The Aso-Kpfa eruption age is constrained at the caldera by its stratigraphic position beneath the AT tephra, as well as several radiocarbon dates obtained from bulk sediment samples of the underlying palaeosols (Miyabuchi, 2009). Paleosol  $^{14}\text{C}$  ages dated by Miyabuchi (2009) can be re-calibrated using IntCal13 to 28,720–29,615 and 31,110–31,940 cal. year BP. In contrast, SG14-2752 is dated using the Lake Suigetsu chronology to 32,647–32,376 cal. year BP (95.4% confidence interval), which is significantly older than the maximum radiocarbon ages. This means that either (i) SG14-2752 represents a pre-Aso-Kpfa eruption at Kusasenrighama/Aso caldera that has not yet been geochemically characterized at source, or (ii) the bulk soil  $^{14}\text{C}$  dates from the paleosol underlying the Aso-Kpfa deposit are not accurate and were perhaps contaminated by younger material. One of the calibrated paleosol ages is younger than the known eruption age of the overlying AT tephra (30,174–29,982 cal. year BP; Albert et al., 2019), which provides further support that the radiocarbon measurements of the soil may not be accurate. Using this evidence we tentatively suggest that SG14-2752 represents the distal fallout of a significant phase of the Aso-Kpfa eruptive sequence that occurred ca. 32.5 ka.

In summary, the Aso-derived tephrostratigraphy preserved at Lake Suigetsu is in agreement with proximal evidence, suggesting that a productive period of activity occurred prior to the AT event. Five separate ash fall events from Aso are preserved in the Lake Suigetsu archive between 35 and 30 ka, indicating that these eruptions dispersed ash over 500 km from source.

### 5.3. Group 2: Aira and Other Sources South of Suigetsu

#### 5.3.1. Aira, Southern Kyushu (Japan)

Aira caldera is situated at the northern end of Kagoshima Bay in southern Kyushu (31°40'N 130°40'E; Figure 1). The flooded collapse structure was formed by the enormous VEI 7 eruption that dispersed the AT ash across the majority of Japan (Aramaki, 1984; Machida & Arai, 2003). The AT eruption ejected approximately 463 km<sup>3</sup> of bulk tephra and is preserved as a >30 cm thick sand-sized tephra (SG06-2650) in Lake Suigetsu (Fukushima & Kobayashi, 2000; Machida & Arai, 2003; Smith et al., 2013). This eruption is most precisely dated using the Lake Suigetsu chronology to 30,174–29,982 IntCal13 year BP (95.4% confidence interval; Albert et al., 2019) and forms the upper boundary of the cryptotephra record presented here. The caldera-forming event began with the Plinian eruption (Osumi pumice fall), which was followed by the Tsumaya and Ito pyroclastic flows (Aramaki, 1984).

In the context of this timeframe (50–30 ka), outcrops from around Aira indicate that the center produced three pyroclastic successions between the 58 ka A-Iwato formation (A-Iw; VEI 6) and the 30 ka AT (VEI 7). These successions are separated by well-developed palaeosols and include the ca. 33 ka Otsuka pumice fall deposit (A-Ot; VEI 4), the ca. 31 ka Fukaminato tephra formation (A-Fm; VEI 5), and the ca. 30 ka Kenashino tephra formation (A-Kn) (Machida & Arai, 2003). Nagaoka et al. (2001) constrained the age of these eruptions using bulk sediment  $^{14}\text{C}$  ages of palaeosols between the A-Ot, A-Fm, and A-Kn units. Here, we incorporate these radiocarbon dates within an OxCal Bayesian phase model (ver. 4.3.2; Bronk Ramsey, 2017) to generate calibrated age estimates for these events. This model is further constrained by inserting the Suigetsu-derived AT eruption age, which is known to post-date these deposits. Using this phase model, the A-Ot eruption is dated to 33,216–30,730 IntCal13 year BP, A-Fm to 30,933–29,865 IntCal13 year BP, and A-Kn to 30,437–29,545 IntCal13 year BP (95.4% confidence interval).

Importantly, volcanic glass from Aira can be distinguished from other sources distributed along the Kyushu SVR arc by their lower Y/HREE and higher Th contents (Figure 5d; Albert et al., 2019). Glasses erupted from Aira are typically homogenous, and trace element compositions are required to robustly distinguish tephra from sequential eruptions. Indeed, Albert et al. (2019) showed that glass compositions of the A-Iw eruption (ca. 58 ka) are subtly elevated in K<sub>2</sub>O (ca. 0.3 wt. %) compared to ash erupted during the 30 ka AT event but could be more confidently discriminated using concentrations of the HFSE. Specifically, the older A-Iw glasses displayed lower Zr content than the AT glasses, most likely relating to a greater degree of zircon fractionation (Figure 6f). Here, geochemical characterization of the intervening Aira eruption units (A-Kn and A-Fm) indicates that they also display the same offsets with respect to the AT eruption deposits, again with

ca. 0.4 wt.% higher  $K_2O$  (Figure 6e) and lower Zr content than the AT tephra. The A-Fm trace element compositions are more heterogeneous in comparison to those of the A-Kn and the older A-Iw unit, with Zr ranging from 70–100 ppm (Figure 6f).

Four cryptotephra layers in the Suigetsu sediments, SG14–3844, SG14–2873, SG14–2856 and SG14–2814, have compositions that are distinctive of those erupted from Aira (Table 1; Figure 5). The trace element compositions of glass from these four cryptotephra layers are more subtly depleted in Zr and more enriched in Th, compared to the AT (Oshumi and Ito) tephra, and are generally more consistent with those of A-Kn, A-Fm, and A-Iw (Figure 6f). While, subtle offsets exist between the trace element compositions of the proximal Aira deposits (A-Kn and A-Fm; Figure 6f) and the distal SG14 ash layers, this is attributed to slight differences in the analytical setup between the two instruments used. Indeed, by correcting the proximal and distal Aira trace element glass data based on differences between the measured and known contents of the StHs6/80-G reference glass, routinely measured on the respective instruments, the chemical similarity between the proximal and distal glasses is clear.

Since these pre-AT tephra units from Aira are compositionally similar we must use the chrono-stratigraphy to facilitate correlations. Since SG14–2856 and SG14–2873 are separated by less than 400 years using the Lake Suigetsu varve chronology, then it is possible that their near-source counterparts would not be separated by a prominent palaeosol. Therefore, it is possible that in the proximal stratigraphy these would be interpreted as separate phases of one of the pre-AT eruptive formations (A-Kn, A-Fm or A-Ot). Based purely on stratigraphic grounds and the eruptive formations recognized at the volcano (Nagaoka et al., 2001), we tentatively suggest that SG14–2814 relates to the A-Kn formation, SG14–2856/SG14–2873 relates to the A-Fm formation, and SG14–3844 is the distal equivalent of the A-Ot formation. While these correlations are not entirely consistent with the existing  $^{14}C$  dates of the palaeosols between the A-Kn, A-Fm, and A-Ot formations (Nagaoka et al., 2001), it is possible that the  $^{14}C$  dates are erroneously young. This is supported by the fact that the paleosol age of the A-Kn deposit (30,437–29,545 cal. year BP) overlaps that of the known age of the AT eruption (30,174–29,982 cal. year BP; Albert et al., 2019), despite these units being separated by a well-developed palaeosol in the proximal sequence. Such soils are also developed between the underlying eruptive units in a period of just 3 ka.

### 5.3.2. Uncorrelated Tephra From Kyushu

Tephra layers SG14–2830 (ca. 34.2 ka), SG14–2995 (ca. 37.4 ka), and SG14–3016 (ca. 37.8 ka) are also attributed to explosive volcanism on the Kyushu arc (Figures 5b and 5c). Considering the compositional overlap, and equivalent shard textures (platy, bubble-walled shards), SG14–2830 and SG14–3016 at least are highly likely to originate from the same source. Trace element compositions obtained for SG14–2830 are less depleted in Nb, Sr, and Eu compared to glass erupted from Aira and therefore more consistent with deposits from Ata and Kikai that are elevated in HFSE (Figures 4c and 4d; Albert et al., 2019). Ata in particular is known to have been active between 50 and 30 ka (Machida & Arai, 2003; Nagaoka et al., 2001), but further proximal samples are required to build geochemical data sets and secure a correlation for these events.

## 5.4. Group 3: Uncorrelated Tephra from Central and Northern Japan

### 5.4.1. Uncorrelated Tephra From Central Honshu

SG14–3336 (ca. 42.0 ka) is compositionally similar to the older visible tephra layer SG06–6634 (ca. 130 ka) identified in the Suigetsu core (Albert et al., 2019; Smith et al., 2013), although glass compositions are ca. 0.5 wt. % lower in  $FeO^T$ . Heterogeneous and medium-K series eruptions are known from stratovolcanoes in central Honshu, including Akagi, Haruna, and Asama (Figures 5e and 5f). Chronologically, the ca. 45 ka eruption of Haruna (Haruna-Hassaki ash; Hr-Hs) and the ca. 44 ka eruption of Akagi (Akagi-Kanuma; Ag-KP) are possible correlatives (Geshu & Oishi, 2011; Suzuki, 1996). However, proximal samples obtained from these units do not span the entire geochemical range of SG14–3336, precluding a robust correlation at this time (Figures 5e and 5f).

### 5.4.2. Uncorrelated Tephra From Hokkaido and the Kurile Arc

SG14–2965 (ca. 36.9 ka) glass shards are very distinctive and contain  $<1$  wt.%  $K_2O$ , suggesting that this deposit was erupted from a source from NE Hokkaido or Kurile arc. The only known low-K source to have dispersed ash to central Honshu is Mashu (Ma-b tephra), situated in eastern Hokkaido (McLean et al., 2018). However, SG14–2965 glass compositions can be distinguished from Mashu tephra (e.g.,

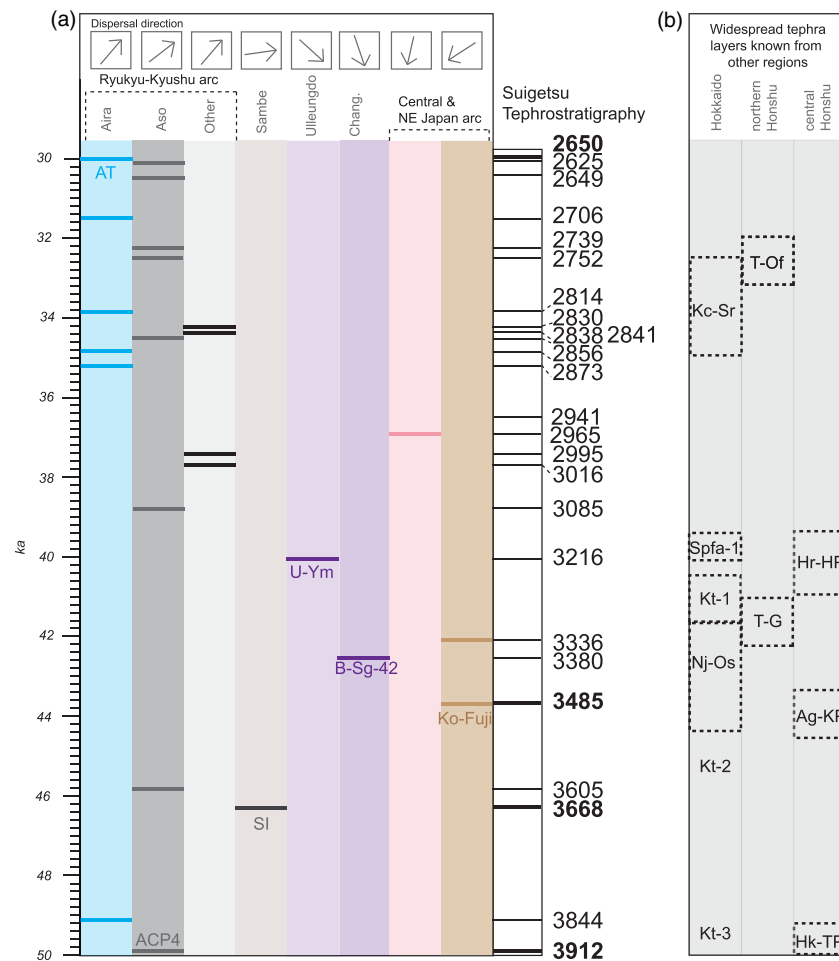


**Figure 7.** (a) Summary of the augmented Lake Suigetsu (SG14) tephrostratigraphy (visible and cryptotephra layers) spanning 50 to 30 ka. The distal tephra layers are correlated to their volcanic sources and, where possible, specific eruptions, using the compositions of the volcanic glass. The Suigetsu sediments preserve evidence of a significant period of activity from centers on the Ryukyu-Kyushu arc (e.g., Aira and Aso) prior to the AT caldera-forming eruption dated to ca. 30 ka. (b) The timing of other key widespread and large magnitude (VEI 7–5) eruptions known from other regions north of Lake Suigetsu, which were not identified in the sediments (data from Machida & Arai, 2003). Approximate eruption ages are shown by dashed boxes, as reported by Suzuki (1996); Machida and Arai (2003); Yamamoto et al. (2010); Geshu and Oishi (2011); Uesawa et al. (2016); Matsu'ura et al. (2017).

Ma-b and older deposits), by CaO (ca. 0.5 wt.% lower) and other minor elements including  $\text{TiO}_2$  (Figures 5e and 5f).

## 6. Discussion

### 6.1. Tempo, Origin, and Dispersal of Ash Fall Events Reaching Central Honshu

The augmented Lake Suigetsu tephrostratigraphic record (50 to 30 ka) indicates that, on average, an ash fall event reached central Honshu at least once every 1,300 years (Figure 7). However, between 39 and 30 ka the average return interval was significantly higher, with at least one eruption recorded every ca. 500 years, which is in close agreement with that observed during the Holocene (McLean et al., 2018). The record is dominated by ash fall events erupted from sources south of Suigetsu on the SVR and CVR ( $n = 18$ ; Figure 7), and most of which ( $n = 8$ ) are derived from explosive activity from Aso (CVR).

Four eruption events are identified from different arc regions in Japan (e.g., central Honshu) and other nearby volcanic settings (Changbaishan and Ulleungdo), which highlights that other sources also have the potential to disperse ash more widely than previously anticipated. Interestingly, these eruption events

are clustered between 45 and 39 ka, when no other ash layers are recorded from productive centers southwest of Suigetsu. However, it is not possible to attribute the cause of this change, due to the number of controlling parameters and preservation biases that affect the presence of cryptotephra layers. For example, this may represent a change in eruption styles and mechanisms (e.g., explosivity; efficient fragmentation of magma; Cassidy et al., 2018) or external differences during eruptions (e.g., wind direction and strength; Carey & Sparks, 1986).

Several volcanoes in northern Honshu and Hokkaido are known to have been very active between 50 and 30 ka (e.g., Towada, Shikotsu); yet, distal ash deposits from these large magnitude events (VEI 5–7) have not been identified in this study of the Suigetsu sediments (Figure 7). It is possible that they are preserved as lower concentrated peaks of glass shards in the sediments or are hidden in the reworked “tails” that follow visible tephra layers. Identifying these markers would be of significant value for tephrochronology and help to further constrain their eruption histories. The identification of other primary cryptotephra peaks in the sediments may be achieved through detailed studies of shard morphologies, supplemented by further geochemical analysis. This was shown to be possible in the Holocene sedimentation, where the distinctive vesicular To-Cu (Towada) shards were clear within the platy K-Ah remobilized glass (McLean et al., 2018).

The Japanese cryptotephra layers identified within the sediments of Lake Suigetsu are the first known distal occurrences of these eruption events. Therefore, further ash deposits between Suigetsu and their sources (e.g., in other high-resolution lake and marine cores) are required to better constrain the magnitude of these events and integrate other eruption stratigraphies. Nevertheless, it is clear that these must have had a VEI of at least 4, in order to have been dispersed as far as Lake Suigetsu (located 300 km from the nearest potential source) and have been preserved as a cryptotephra layer. Cryptotephra ash fall events are likely to be thin and perhaps of limited consequence so far from source, but such fine ash (typically  $<80\ \mu\text{m}$ ) may have implications for air traffic, air and water quality, and critical infrastructure (e.g., Horwell & Baxter, 2006).

## 6.2. Constrained Eruption Chronology for Aso and Aira

The Suigetsu tephrostratigraphy provides detailed insight into the behavior of two of the most active calderas in Japan, Aso and Aira, which are central to hazard assessments for Japan and even possible candidates for the next VEI 7 eruption (Newhall et al., 2018). Here, we confirm that both centers were very active between 50 and 30 ka (as informed by their proximal stratigraphies), producing moderate to large explosive events within short temporal scales (ca. 300 years for both). Almost all of these eruptions have yet to be the subject of detailed petrological investigations, so the glass compositions and constrained eruption ages allow a new insight and comparisons into the magma generation and storage pre- (Aira) and post- (Aso) caldera-forming events.

Prior to the AT eruption (VEI 7; Machida & Arai, 2003) of Aira, the Suigetsu record indicates that at least four large eruption events occurred and are dated to ca. 33.8, 34.8, 35.2, and 49.2 ka (Table 1; Figure 7). The Suigetsu chronology also indicates that these eruptions occurred as frequently as 3,600 years before the enormous AT event. These erupted characteristically high silicic glass compositions (75.5–78.9 wt.%  $\text{SiO}_2$ ) that are compositionally similar on major elements (Albert et al., 2019; Machida & Arai, 2003), but we show that they can be geochemically distinguished from the AT ash using their trace element compositions (e.g., Zr, Y, and Th).

The Suigetsu sediments indicate that Aso erupted compositionally different magmas through time, ranging from rhyolitic to andesitic in composition and producing at least eight widespread tephra units over 20 ka (Table 1; Figure 7). Furthermore, Aso was also very active prior to the AT eruption at ca. 30 ka, with at least one eruption every 600 years between ca. 32.6 and 30.3 ka. The bulk volumes estimated for the Aso eruption events (Miyabuchi, 2009, 2011) in some cases are small; yet, they are preserved over 600 km from the vent. This could imply that perhaps the eruption volumes are underestimated, the transport mechanism is highly efficient, and/or the eruptions generated very fine ash suitable for widespread ash dispersal.

## 7. Conclusions

New insights into the frequency and timing of East Asian volcanism between 50 and 30 ka are elucidated through the identification of non-visible (cryptotephra) layers preserved in the laminated (varved) sediments of Lake Suigetsu (Japan). Four times more cryptotephra layers are preserved relative to visible layers,



meaning that this tephrostratigraphy provides an unprecedented record of ash that has been dispersed over central Honshu. Major and trace element compositions of the glass shards allow most of these distal tephra to be correlated to their volcanic source; however, additional datasets from proximal outcrops are pivotal to integrate these records and learn more about these individual eruption events.

Of the 25 ash layers presented in the augmented tephrostratigraphy, 19 of these were dispersed from eruptive centres southwest of Suigetsu, which is unsurprising considering the prevailing westerly winds. However, the record indicates that other sources have the potential to reach central Honshu, including Ulleungdo (500 km NW of Suigetsu) and Changbaishan (1,000 km NW). Explosive activity from Aso and Aira is most frequently recorded in the record and indicates that these calderas were very active between 35 and 30 ka. Aso erupted compositionally different magmas through time, producing eight widespread events over 20 ka. Here, we also show that Aira erupted explosively 1.3 ka before the catastrophic VEI 7 caldera-forming eruption that blanketed Japan in the AT ash.

### Acknowledgments

The SG14 (formally “Fukui-SG14”) sediment coring campaign was funded by the Fukui Prefectural government, and the coring was conducted by the team of Seibushisui Co. Ltd. Japan, led by Mr. Atsumi Kitamura. KAKENHI grants by MEXT, Japan (15H021443 and 18H03744 to TN), and grants by Casio Science Promotion Foundation were used to purchase laboratory equipment and consumables during the project. Trace element analysis was funded by the Japan Society for the Promotion of Science (JSPS) 2018 Summer Program. DM was funded by NERC (grant: NE/L002612/1) and part of the Environmental Research Doctoral Training Program at the University of Oxford. PGA was supported by an Early Career Fellowship from the Leverhulme Trust (grant: ECF-2014-438) and through a UK Research and Innovation Future Leaders Fellowship (grant: MR/S035478/1). RAS was supported by an Early Career Fellowship from the Leverhulme Trust (grant: ECF-2015-396). The authors would like to thank Jenni L. Hopkins, Eliza Cook and another anonymous reviewer for their detailed and constructive reviews. Data sets for this research are archived in the University of Oxford Repository (ORA-Data; DOI: <https://doi.org/10.5287/bodleian:BpKwxb90Q>) and are also included in the Supplementary Information.

### References

- Albert, P. G., Smith, V. C., Suzuki, T., McLean, D., Tomlinson, E. L., Miyabuchi, Y., et al. (2019). Geochemical characterisation of the widespread Japanese tephrostratigraphic markers and correlations to the Lake Suigetsu sedimentary archive (SG06 core). *Quaternary Geochronology*, 52, 103–131. <https://doi.org/10.1016/j.quageo.2019.01.005>
- Albert, P. G., Smith, V. C., Suzuki, T., Tomlinson, E. L., Nakagawa, T., McLean, D., et al. (2018). Constraints on the frequency and dispersal of explosive eruptions at Sambe and Daisen volcanoes (South-West Japan Arc) from the distal Lake Suigetsu record (SG06 core). *Earth-Science Reviews*, 185, 1004–1028. <https://doi.org/10.1016/j.earscirev.2018.07.003>
- Allan, A. S., Baker, J. A., Carter, L., & Wysoczanski, R. J. (2008). Reconstructing the quaternary evolution of the world's most active silicic volcanic system: Insights from an ~1.65 Ma deep ocean tephra record sourced from Taupo volcanic zone, New Zealand. *Quaternary Science Reviews*, 27(25–26), 2341–2360. <https://doi.org/10.1016/j.quascirev.2008.09.003>
- Aoki, K. (2008). Revised age and distribution of ca. 87ka Aso-4 tephra based on new evidence from the northwest Pacific Ocean. *Quaternary International*, 178(1), 100–118. <https://doi.org/10.1016/j.quaint.2007.02.005>
- Aramaki, S. (1984). Formation of the Aira caldera, southern Kyushu, ~ 22,000 years ago. *Journal of Geophysical Research*, 89(B10), 8485–8501. <https://doi.org/10.1029/JB089iB10p08485>
- Blockley, S. P. E., Pyne-O'Donnell, S. D. F., Lowe, J. J., Matthews, I. P., Stone, A., Pollard, A. M., et al. (2005). A new and less destructive laboratory procedure for the physical separation of distal glass tephra shards from sediments. *Quaternary Science Reviews*, 24(16–17), 1952–1960. <https://doi.org/10.1016/j.quascirev.2004.12.008>
- Bourne, A. J., Cook, E., Abbott, P. M., Seierstad, I. K., Steffensen, J. P., Svensson, A., et al. (2015). A tephra lattice for Greenland and a reconstruction of volcanic events spanning 25–45 ka b2k. *Quaternary Science Reviews*, 118, 122–141. <https://doi.org/10.1016/j.quascirev.2014.07.017>
- Bronk Ramsey, C. (2008). Deposition models for chronological records. *Quaternary Science Reviews*, 27(1–2), 42–60. <https://doi.org/10.1016/j.quascirev.2007.01.019>
- Bronk Ramsey, C. (2017). OxCal Project, Version 4.3. Retrieved December 2017. <https://c14.arch.ox.ac.uk/oxcal/OxCal.html>
- Bronk Ramsey, C., Heaton, T., & Schlögl, G. (2020). Reanalysis of the atmospheric radiocarbon calibration record from Lake Suigetsu, Japan. *Radiocarbon*, 1–11. <https://doi.org/10.1017/RDC.2020.18>
- Bronk Ramsey, C., Staff, R. A., Bryant, C. L., Brock, F., Kitagawa, H., Van Der Plicht, J., et al. (2012). A complete terrestrial radiocarbon record for 11.2 to 52.8 kyr BP. *Science*, 338(6105), 370–374. <http://doi.org/10.1126/science.1226660>
- Carey, S., & Sparks, R. S. J. (1986). Quantitative models of the fallout and dispersal of tephra from volcanic eruption columns. *Bulletin of Volcanology*, 48(2–3), 109–125. <https://doi.org/10.1007/BF01046546>
- Cassidy, M., Manga, M., Cashman, K., & Bachmann, O. (2018). Controls on explosive-effusive volcanic eruption styles. *Nature Communications*, 9(1), 2839. <https://doi.org/10.1038/s41467-018-05293-3>
- Chen, X. Y., Blockley, S. P., Tarasov, P. E., Xu, Y. G., McLean, D., Tomlinson, E. L., et al. (2016). Clarifying the distal to proximal tephrochronology of the millennium (B-Tm) eruption, Changbaishan volcano, Northeast China. *Quaternary Geochronology*, 33, 61–75. <https://doi.org/10.1016/j.quageo.2016.02.003>
- Chen, X. Y., McLean, D., Blockley, S., Tarasov, P., Xu, Y. G., & Menzies, M. (2019). Developing a Holocene tephrostratigraphy for northern Japan using the sedimentary record from Lake Kushi, Rebun Island. *Quaternary Science Reviews*, 215, 272–292. <https://doi.org/10.1016/j.quascirev.2019.05.017>
- Cook, E., Portnyagin, M., Ponomareva, V., Bazanova, L., Svensson, A., & Garbe-Schönberg, D. (2018). First identification of cryptotephra from the Kamchatka peninsula in a Greenland ice core: Implications of a widespread marker deposit that links Greenland to the Pacific northwest. *Quaternary Science Reviews*, 181, 200–206. <https://doi.org/10.1016/j.quascirev.2017.11.036>
- Fukushima, D., & Kobayashi, T. (2000). Mechanism of generation and emplacement of the Taramizu pyroclastic flow associated with Osumi plinian eruption from Aira caldera, Japan. *Bulletin of Volcanological Society of Japan*, 45(4), 225–240.
- Furuta, T., Fujioka, K., & Arai, F. (1986). Widespread submarine tephra around Japan—Petrographic and chemical properties. *Marine Geology*, 72(1–2), 125–142. [https://doi.org/10.1016/0025-3227\(86\)90103-9](https://doi.org/10.1016/0025-3227(86)90103-9)
- Geshu, N., & Oishi, M. (2011). The <sup>14</sup>C ages of the late Pleistocene–Holocene volcanic products erupted from the Haruna volcano. *Bulletin of the Geological Survey of Japan*, 62, 177–183.
- Horwell, C. J., & Baxter, P. J. (2006). The respiratory health hazards of volcanic ash: A review for volcanic risk mitigation. *Bulletin of Volcanology*, 69(1), 1–24. <https://doi.org/10.1007/s00445-006-0052-y>
- Jensen, B. J., Pyne-O'Donnell, S., Plunkett, G., Froese, D. G., Hughes, P. D., Sigl, M., et al. (2014). Transatlantic distribution of the Alaskan white river ash. *Geology*, 42(10), 875–878. <https://doi.org/10.1130/G35945.1>
- Jochum, K. P., Stoll, B., Herwig, K., Willbold, M., Hofmann, A. W., Amini, M., et al. (2006). MPI-DING reference glasses for in situ microanalysis: New reference values for element concentrations and isotope ratios. *Geochemistry, Geophysics, Geosystems*, 7, Q02008. <https://doi.org/10.1029/2005GC001060>

- Kaneko, K., Inoue, K., Koyaguchi, T., Yoshikawa, M., Shibata, T., Takahashi, T., & Furukawa, K. (2015). Magma plumbing system of the Aso-3 large pyroclastic eruption cycle at Aso volcano, Southwest Japan: Petrological constraint on the formation of a compositionally stratified magma chamber. *Journal of Volcanology and Geothermal Research*, 303, 41–58. <https://doi.org/10.1016/j.jvolgeores.2015.07.016>
- Kimura, J. I., & Chang, Q. (2012). Origin of the suppressed matrix effect for improved analytical performance in determination of major and trace elements in anhydrous silicate samples using 200 nm femtosecond laser ablation sector-field inductively coupled plasma mass spectrometry. *Journal of Analytical Atomic Spectrometry*, 27(9), 1549–1559. <https://doi.org/10.1039/C2JA10344C>
- Kimura, J. I., Nagahashi, Y., Satoguchi, Y., & Chang, Q. (2015). Origins of felsic magmas in Japanese subduction zone: Geochemical characterizations of tephra from caldera-forming eruptions < 5 ma. *Geochemistry, Geophysics, Geosystems*, 16, 2147–2174. <https://doi.org/10.1002/2015GC005854>
- Kitagawa, H., & van der Plicht, H. (1998a). A 40,000-year varve chronology from Lake Suigetsu, Japan: Extension of the C-14 calibration curve. *Radiocarbon*, 40(1), 505–515. <https://doi.org/10.1017/S0033822200018385>
- Kitagawa, H., & van der Plicht, H. (1998b). Atmospheric radiocarbon calibration to 45,000 yr B.P.: Late glacial fluctuations and Cosmogenic isotope production. *Science*, 279(5354), 1187–1190. <https://doi.org/10.1126/science.279.5354.1187>
- Kitagawa, H., & van der Plicht, J. (2000). Atmospheric radiocarbon calibration beyond 11,900 cal BP from Lake Suigetsu laminated sediments. *Radiocarbon*, 42(3), 370–381. <https://doi.org/10.1017/S0033822200030319>
- Kiyosugi, K., Connor, C., Sparks, R. S. J., Croswell, H. S., Brown, S. K., Siebert, L., et al. (2015). How many explosive eruptions are missing from the geologic record? Analysis of the quaternary record of large magnitude explosive eruptions in Japan. *Journal of Applied Volcanology*, 4(1), 1–15. <https://doi.org/10.1186/s13617-015-0035-9>
- Lane, C. S., Brauer, A., Martín-Puertas, C., Blockley, S. P., Smith, V. C., & Tomlinson, E. L. (2015). The Late Quaternary tephrostratigraphy of annually laminated sediments from Meerfelder maar, Germany. *Quaternary Science Reviews*, 122, 192–206. <https://doi.org/10.1016/j.quascirev.2015.05.025>
- Lane, C. S., Cullen, V. L., White, D., Bramham-Law, C. W. F., & Smith, V. C. (2014). Cryptotephra as a dating and correlation tool in archaeology. *Journal of Archaeological Science*, 42, 42–50. <https://doi.org/10.1016/j.jas.2013.10.033>
- Le Bas, M. J., Le Maitre, R. W., Streckeisen, A., & Zanettin, B. (1986). A chemical classification of volcanic rocks based on the total alkali-silica diagram. *Journal of Petrology*, 27(3), 745–750. <https://doi.org/10.1093/petrology/27.3.745>
- Lim, C., Toyoda, K., Ikehara, K., & Peate, D. W. (2013). Late Quaternary tephrostratigraphy of Baegdusan and Ulleung volcanoes using marine sediments in the Japan Sea/East Sea. *Quaternary Research*, 80(1), 76–87. <https://doi.org/10.1016/j.yqres.2013.04.002>
- Machida, H., & Arai, F. (1983). Extensive ash falls in and around the sea of Japan from large late Quaternary eruptions. *Journal of Volcanology and Geothermal Research*, 18(1–4), 151–164.
- Machida, H., & Arai, F. (2003). *Atlas of tephra in and around Japan* (Revised ed.). Tokyo: Tokyo University Press.
- Mackay, H., Hughes, P. D., Jensen, B. J., Langdon, P. G., Pyne-O'Donnell, S. D., Plunkett, G., et al. (2016). A mid to late Holocene cryptotephra framework from eastern North America. *Quaternary Science Reviews*, 132, 101–113. <https://doi.org/10.1016/j.quascirev.2015.11.011>
- Mahony, S. H., Sparks, R. S. J., Wallace, L. M., Engwell, S. L., Scourse, E. M., Barnard, N. H., et al. (2016). Increased rates of large-magnitude explosive eruptions in Japan in the late Neogene and quaternary. *Geochemistry, Geophysics, Geosystems*, 17, 2467–2479. <https://doi.org/10.1002/2016GC006362>
- Marshall, M., Schlolaut, G., Nakagawa, T., Lamb, H., Brauer, A., Staff, R., et al. (2012). A novel approach to varve counting using  $\mu$ XRF and X-radiography in combination with thin-section microscopy, applied to the late glacial chronology from Lake Suigetsu, Japan. *Quaternary Geochronology*, 13, 70–80. <https://doi.org/10.1016/j.quageo.2012.06.002>
- Matsuura, T., Kimura, J. I., Chang, Q., & Komatsubara, J. (2017). Using tephrostratigraphy and cryptotephrostratigraphy to re-evaluate and improve the middle Pleistocene age model for marine sequences in Northeast Japan (Chikyu C9001C). *Quaternary Geochronology*, 40, 129–145. <https://doi.org/10.1016/j.quageo.2016.11.001>
- McLean, D., Albert, P. G., Nakagawa, T., Staff, R., Suzuki, T., & Smith, V. C. (2016). Identification of the Changbaishan 'Millennium' (B-Tm) eruption deposit in the Lake Suigetsu (SG06) sedimentary archive, Japan: Synchronisation of hemispheric-wide palaeoclimate archives. *Quaternary Science Reviews*, 150, 301–307. <https://doi.org/10.1016/j.quascirev.2016.08.022>
- McLean, D., Albert, P. G., Nakagawa, T., Suzuki, T., Staff, R., Yamada, K., et al. (2018). Integrating the Holocene tephrostratigraphy for East Asia using a high-resolution cryptotephra study from Lake Suigetsu (SG14 core), Central Japan. *Quaternary Science Reviews*, 183, 36–58. <https://doi.org/10.1016/j.quascirev.2017.12.013>
- McLean, D., Albert, P. G., Suzuki, T., Nakagawa, T., Kimura, J. I., Chang, Q., et al. (2020). Refining the eruptive history of Ulleungdo and Changbaishan volcanoes (East Asia) over the last 86 kys using distal sedimentary records. *Journal of Volcanology and Geothermal Research*, 389(150), 301–307.
- Miyabuchi, Y. (2009). A 90,000-year tephrostratigraphic framework of Aso volcano, Japan. *Sedimentary Geology*, 220(3–4), 169–189. <https://doi.org/10.1016/j.sedgeo.2009.04.018>
- Miyabuchi, Y. (2011). Post-caldera explosive activity inferred from improved 67–30 ka tephrostratigraphy at Aso Volcano, Japan. *Journal of Volcanology and Geothermal Research*, 205(3–4), 94–113. <https://doi.org/10.1016/j.jvolgeores.2011.05.004>
- Miyabuchi, Y., Hoshizumi, H., Takada, H., Watanabe, K., & Xu, S. (2003). Pumice-fall deposits from Aso volcano during the past 90,000 years, southwestern Japan. *Bulletin of the Volcanological Society of Japan*, 48, 195–214. (in Japanese with English abstract)
- Miyabuchi, Y., Hoshizumi, H., & Watanabe, K. (2004). Late Pleistocene tephrostratigraphy of Aso volcano, southwestern Japan, after deposition of AT ash. *Bulletin of the Volcanological Society of Japan*, 49, 51–64. (in Japanese with English abstract)
- Nagaoka, S., Okuno, M., & Arai, F. (2001). Tephrostratigraphy and eruptive history of the Aira caldera volcano during 100–30 ka, Kyushu, Japan. *Journal of the Geological Society of Japan*, 107(7), 432–450. <https://doi.org/10.5575/geosoc.107.432>
- Nakagawa, T., Kitagawa, H., Yasuda, Y., Tarasov, P. E., Gotanda, K., Sawai, Y. (2005). Pollen/event stratigraphy of the varved sediment of Lake Suigetsu, central Japan from 15,701 to 10,217 SG vyr BP (Suigetsu varve years before present): Description, interpretation, and correlation with other regions. *Quaternary Science Reviews*, 24, (14–15), 1691–1701. <https://doi.org/10.1016/j.quascirev.2004.06.022>
- Moriwaki, H., Nakamura, N., Nagasako, T., Lowe, D. J., Sangawa, T. (2016). The role of tephra in developing a high-precision chronostratigraphy for palaeoenvironmental reconstruction and archaeology in southern Kyushu, Japan, since 30,000 cal. BP: An integration. *Quaternary International*, 397, 79–92. <https://doi.org/10.1016/j.quaint.2015.05.069>
- Nakagawa, T., Gotanda, K., Haraguchi, T., Danhara, T., Yonenobu, H., Brauer, A., et al. (2012). SG06, a perfectly continuous and varved sediment core from Lake Suigetsu, Japan: Stratigraphy and potential for improving the radiocarbon calibration model and understanding of late Quaternary climate changes. *Quaternary Science Reviews*, 36, 164–176. <https://doi.org/10.1016/j.quascirev.2010.12.013>

- Nakamura, Y. (2016). Stratigraphy, distribution, and petrographic properties of Holocene tephra in Hokkaido, northern Japan. *Quaternary International*, 397, 52–62. <https://doi.org/10.1016/j.quaint.2015.07.056>
- Newhall, C., Self, S., & Robock, A. (2018). Anticipating future volcanic Explosivity index (VEI) 7 eruptions and their chilling impacts. *Geosphere*, 14(2), 572–603. <https://doi.org/10.1130/GES01513.1>
- Okuno, M., Torii, M., Yamada, K., Shinozuka, Y., Danhara, T., Gotanda, K., et al. (2011). Widespread tephra in sediments from lake Ichino-Megata in northern Japan: Their description, correlation and significance. *Quaternary International*, 246(1–2), 270–277. <https://doi.org/10.1016/j.quaint.2011.08.015>
- Ono, K. (1989). Rocks of Aso volcano. Seminar of 1989 Fall Meeting of the Volcanological Society of Japan, 8–14 (in Japanese).
- Reimer, P. J., Bard, E., Bayliss, A., Beck, J. W., Blackwell, P. G., Ramsey, C. B., et al. (2013). IntCal13 and Marine13 radiocarbon age calibration curves 0–50,000 years cal BP. *Radiocarbon*, 55(4), 1869–1887.
- Schindlbeck, J. C., Kutterolf, S., Straub, S. M., Andrews, G. D. M., Wang, K.-L., Mleneck-Vautravets, M. J. (2018). One Million Years tephra record at IODP Sites U1436 and U1437: Insights into explosive volcanism from the Japan and Izu arcs. *Island Arc*, 27(3), e12244. <https://doi.org/10.1111/iar.12244>
- Schlout, G., Brauer, A., Marshall, M. H., Nakagawa, T., Staff, R. A., Bronk Ramsey, C., Lamb, H. F., et al. (2014). Event layers in the Japanese Lake Suigetsu 'SG06' sediment core: description, interpretation and climatic implications. *Quaternary Science Reviews*, 83, 157–170. <https://doi.org/10.1016/j.quascirev.2013.10.026>
- Schlout, G., Marshall, M. H., Brauer, A., Nakagawa, T., Lamb, H. F., Staff, R., et al. (2012). An automated method for varve interpolation and its application to the late glacial chronology from Lake Suigetsu, Japan. *Quaternary Geochronology*, 13(4), 52–69. [https://doi.org/10.2458/azu\\_js\\_rc.55.16947](https://doi.org/10.2458/azu_js_rc.55.16947)
- Schlout, G., Staff, R., Brauer, A., Lamb, H. F., Marshall, M. H., Ramsey, C. B., & Nakagawa, T. (2018). An extended and revised Lake Suigetsu varve chronology from ~50 to ~10 ka BP based on detailed sediment micro-facies analyses. *Quaternary Science Reviews*, 200, 351–366. <https://doi.org/10.1016/j.quascirev.2018.09.021>
- Simkin, T., & Siebert, L. (2000). Earth's volcanoes and eruptions: An overview. In H. Sigurdsson, et al. (Eds.), *Encyclopedia of Volcanoes* (pp. 249–261). San Diego: Academic Press.
- Smith, V. C., Mark, D. F., Staff, R., Blockley, S. P. E., Bronk-Ramsey, C., Bryant, C. L., et al. (2011). Toward establishing precise Ar/Ar chronologies for Late Pleistocene palaeoclimate archives: An example from the Lake Suigetsu (Japan) sedimentary record. *Quaternary Science Reviews*, 30(21–22), 2845–2850. <https://doi.org/10.1016/j.quascirev.2011.06.020>
- Smith, V. C., Staff, R., Blockley, S. P. E., Bronk Ramsey, C., Nakagawa, T., Mark, D. F., et al. (2013). Identification and correlation of visible tephra in the Lake Suigetsu SG06 sedimentary archive, Japan: Chronostratigraphic markers for synchronising of east Asian/West Pacific palaeoclimatic records across the last 150 ka. *Quaternary Science Reviews*, 61, 121–137. <https://doi.org/10.1016/j.quascirev.2013.01.026>
- Staff, R., Bronk Ramsey, C., Bryant, C. L., Brock, F., Payne, R. L., Schlout, G., et al. (2011). New 14C determinations from Lake Suigetsu, Japan: 12,000 to 0 cal. BP. *Radiocarbon*, 53(3), 511–528. <https://doi.org/10.1017/S0033822200034627>
- Staff, R., Nakagawa, T., Schlout, G., Marshall, M. H., Brauer, A., Lamb, H. F., et al. (2013a). The multiple chronological techniques applied to the Lake Suigetsu SG06 sediment core, Central Japan. *Boreas*, 42(2), 259–266. <https://doi.org/10.1111/j.1502-3885.2012.00278.x>
- Staff, R., Schlout, G., Ramsey, C. B., Brock, F., Bryant, C. L., Kitagawa, H., et al. (2013b). Integration of the old and new Lake Suigetsu (Japan) terrestrial radiocarbon calibration data sets. *Radiocarbon*, 55(4), 2049–2058. [https://doi.org/10.2458/azu\\_js\\_rc.v55i2.16339](https://doi.org/10.2458/azu_js_rc.v55i2.16339)
- Sun, C., You, H., Liu, J., Li, X., Gao, J., & Chen, S. (2014). Distribution, geochemistry and age of the Millennium eruptives of Changbaishan volcano, Northeast China—A review. *Frontiers of Earth Science*, 8(2), 216–230. <https://doi.org/10.1007/s11707-014-0419-x>
- Sun, S. S., & McDonough, W. F. (1989). Chemical and isotopic systematics of oceanic basalts: Implications for mantle composition and processes. *Geological Society, London, Special Publications*, 42(1), 313–345. <https://doi.org/10.1144/GSL.SP.1989.042.01.19>
- Suzuki, T. (1996). Discharge rates of fallout tephra and frequency of plinian eruptions during the last 400,000 years in the southern Northeast Japan arc. *Quaternary International*, 34, 79–87. [https://doi.org/10.1016/1040-6182\(95\)00071-2](https://doi.org/10.1016/1040-6182(95)00071-2)
- Tada, R. (1999). Late Quaternary paleoceanography of the Japan Sea. *The Quaternary Research (Daiyonki-Kenkyu)*, 38(3), 216–222. <https://doi.org/10.4116/jaqua.38.216>
- Takada, H. (1989). Preliminary report on tephra from Aso central cones. *Journal of the Kumamoto Geoscience Association*, 90, 8–11. (in Japanese)
- Tomlinson, E. L., Thordarson, T., Müller, W., Thirlwall, M., & Menzies, M. A. (2010). Microanalysis of tephra by LA-ICP-MS—Strategies, advantages and limitations assessed using the Thorsmörk ignimbrite (southern Iceland). *Chemical Geology*, 279(3–4), 73–89. <https://doi.org/10.1016/j.chemgeo.2010.09.013>
- Turney, C. S. (1998). Extraction of rhyolitic component of Vedde microtephra from minerogenic lake sediments. *Journal of Paleolimnology*, 19(2), 199–206. <https://doi.org/10.1023/A:1007926322026>
- Uesawa, S., Nakagawa, M., & Umetsu, A. (2016). Explosive eruptive activity and temporal magmatic changes at Yotei volcano during the last 50,000 years, Southwest Hokkaido, Japan. *Journal of Volcanology and Geothermal Research*, 325, 27–44. <https://doi.org/10.1016/j.jvolgeores.2016.06.008>
- van der Bilt, W. G., Lane, C. S., & Bakke, J. (2017). Ultra-distal Kamchatkan ash on Arctic Svalbard: Towards hemispheric cryptotephra correlation. *Quaternary Science Reviews*, 164, 230–235. <https://doi.org/10.1016/j.quascirev.2017.04.007>
- Watanabe, K., Ono, K., & Hiratsuka, S. (1982). Pumice eruption at Kusasenrigahama volcano. *Bulletin of the Volcanological Society of Japan*, 27, 337–339. (in Japanese)
- Yamamoto, T., Itho, J., Nakagawa, M., Hasegawa, T., & Kishimoto, H. (2010). 14C ages for the ejecta from Kutcharo and Mashu caldera, eastern Hokkaido, Japan. *Bulletin of the Geological Survey of Japan*, 61(5–6), 161–170. (in Japanese with English abstract)